DETECTION OF A SINGLE MOLECULE IN A CAPILLARY BY LASER-INDUCED FLUORESCENCE

By

YUAN-HSIANG LEE

A DISSERTATION PRESENTED TO THE GRADUATE SCHOOL
OF THE UNIVERSITY OF FLORIDA IN PARTIAL FULFILLMENT
OF THE REQUIREMENTS FOR THE DEGREE OF
DOCTOR OF PHILOSOPHY

UNIVERSITY OF FLORIDA

1994

ACKNOWLEDGMENTS

I would like to thank my research advisor, Prof James D Winefordner, for giving me freedom and guidance to pursue the work described in this dissertation His enthusiasm, hard work, and perseverance will always be with me It has been e pleasure and an inspiration to work in his "world-class" research group

Thanks go to Dr Benjamin W Smith for his help in the laboratory as well as many innovative ideas and much good advice On a more practical nature, I would like to express my sincere gratitude to Dr. Dennis Hueber for his knowledge in experimental design and computer data acquisition. I would also want to thank Dr Mark C Yang and Mr Chi-Hse Teng in the Department of Statistics to provide the mathematical model for data analysis I also would like to thank my predecessor, Dr Steve J Lehotay, for his pioneer approach to this work Thanks go to Dr Robert Kennedy for the discussion related to some technical problems and practical applications of this research My great appreciation extends to Dr Martin Vala Dr Venice Young, and Dr Eric Allen for their supervision during my stay at the University of Florida

I also would like to thank all members of the group, past and present, for their friendship. I thank the help from the senior undergraduate co-worker, Russell Maus, who received the award for his undergraduate research related to this

study. Thanks go to the department machinists, Chester Eastman, Vernon Cook, and Dalley Burch, for the construction of equipment used in this research.

I acknowledge the Division of Sponsored Research at the University of Florida for the graduate assistantship and some financial support on this work.

I would like to express thanks for the invaluable friendship from Chiu-Chin (Sally) Chang and for her support, kindness, and understanding.

I would especially like to thank my parents for encouraging me to expand my education far away from home. Their endless love and support have meant so much in my life. I dedicate this study to my parents.

TABLE OF CONTENTS

Abstract of Dissertation Presented to the Graduate School
of the University of Florida in Partial Fulfillment of the
Requirements for the Doctor of Philosophy

DETECTION OF A SINGLE MOLECULE IN A CAPILLARY
BY LASER-INDUCED FLUORESCENCE

By

YUAN-HSIANG LEE

AUGUST 1994

Chairperson: James D. Winefordner
Major Department: Chemistry

The objective of this dissertation is to develop a novel laser excited spectrometric method to reliably detect a single molecule in a flowing stream which is confined in a capillary. The laser is tuned to the rubidium atomic absorption line at 780.023 nm and focused onto the uncoated part of the capillary. A heated rubidium metal vapor filter based on the resonance absorption of an atomic vapor absorbs the laser specular scatter while passing the molecular fluorescence. The fluorescence is then focused by a microscope objective into an optical fiber which is prealigned to the detector. Raman scatter is reduced by flowing the molecules in the small probe volume. Background fluorescence is virtually eliminated by working in the near-infrared. The excitation source is a Ti:sapphire laser with a linewidth narrower than the rubidium atomic absorption bandwidth. The detector

is a single photon avalanche photodiode with high photon detection efficiency and low dark count rate

The concept of single molecule detection is addressed in terms of limit of detection, limit of guarantee, intrinsic noise, extrinsic noise, as well as detection efficiency and measurement efficiency. The generalized Lorentzian approximation for Voigt line shape is used to simulate the absorption profile of the rubidium metal vapor filter at different temperatures. The absorbance of the rubidium metal vapor filter at 170 °C is measured to be 8.

A photostability study of IR140 molecules dissolved in methanol is evaluated to optimize laser power and molecular transit time in the probe volume. The linear range of calibration curve is from 1.5×10^{-12} M to 1.5×10^{-8} M which corresponds to 1 to 10,000 molecules per transit time in the probe volume. A statistical model based on the Poisson distribution has been successfully applied to describe the detected events coming from single molecules. A weighted quadratic summing filter is used to extract the individual photon bursts from single molecules. The average number of signal counts from single IR140 molecule is estimated to be 5.4, 6.6, and 9.1 for laser powers of 50 mW, 100 mW, and 150 mW

CHAPTER 1
INTRODUCTION

Overview

There has been a concerted effort to push the detection limit of molecules in solution to single molecule level. Detection of a single molecule in solution has been achieved with a variety of experimental schemes, all involving efficient laser excitation and fluorescent detection. The development of the lasers makes it feasible to detect and identify individual molecules by laser-induced fluorescence (LIF) photon burst detection. As a molecule passes through a focused laser beam, it is repeatedly cycled between the ground electronic state and the excited electronic state with the emission of a photon on each cycle (Figure 1-1). The photon burst size can be thousands or hundreds of thousands of photons, ultimately limited by the photostability of the molecule.

This dissertation will address an important concept in single molecule detection. That is how to improve the efficiency of detecting all the molecules in a sample in contrast to just those that pass through the probe volume. In previous experiments for single molecule detection, most of the molecules did not pass through the excitation laser beam and as a result the overall detection efficiency was low. Our unique approach is to confine the molecules in a capillary tube, to

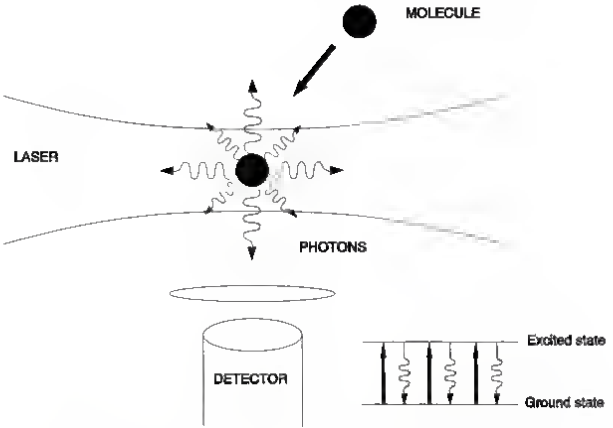

Figure 1-1 Schematic representation of photon-burst detection of single molecules

irradiate the entire internal diameter of the capillary with the excitation laser beam, and to absorb the laser specular scatter with a metal vapor filter.

Sensitive fluorescence detection in solution is limited by the background noise sources from the optics and the solvent. The central problem of isolating the molecular fluorescence from background luminescence and Raman scatter is overcome by reducing the probe volume to the smallest possible size. The reduction in the probe volume can be achieved by optically restricting the illuminated and/or observed volume, by physically decreasing the size of sample confinement, or by a combination of these techniques. Various experimental schemes, such as sheath flow cell and electrodynamic levitated microdroplets have been applied as the sample confinement for single molecule detection (SMD).

Historical Background

Gas-phase detection of single atoms by resonance ionization and fluorescence spectroscopy was demonstrated by Hurst et al.[1] and Pan et al.[2] Single molecules doped in solid matrices have been detected at low temperatures by Moerner et al.,[3] Orrit et al.,[4] and Betzig et al.[5] Detection of a single molecule in liquid solution at room temperature presents many new challenges and applications. A history of the approach to single molecule detection in solution is given in Figure 1-2. The pioneering work of Hirschfeld has demonstrated that LIF has the sensitivity of detecting a small number of fluorescent molecules.[6] Dovichi et al. (Keller's group at Los Alamos National Laboratory) modified the flow

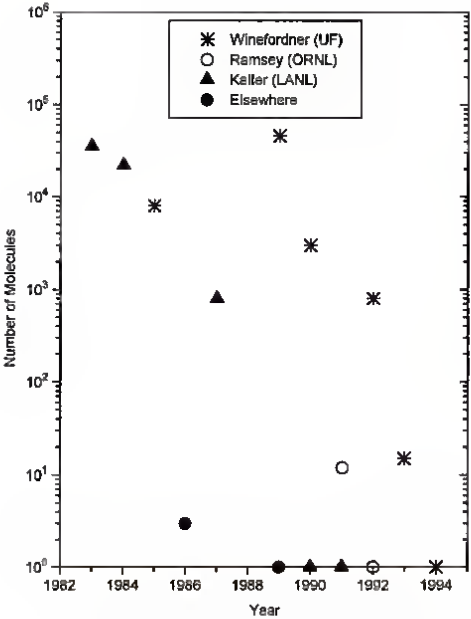

Figure 1-2 History of single molecule detection in solution

cytometer and was able to detect attogram quantities of aqueous rhodamine 6G (R-6G) by LIF analysis. A detection limit of 28 attograms (35 000 molecules) was obtained. The detection limit in concentration was 1.4×10^{-12} M. During the 1-sec measurement period, the total volume sampled was 0.42 μL. On average, only half of a R-6G molecule was presented in the 6 pL probe volume. Dovichi et al. (Keller's group) suggested LIF as an approach for SMD in solution.[7] Recognizing that a greater S/N could be obtained by reduction in the effective sample volume, they achieved a detection limit of 22,000 R-6G molecules by using a hydrodynamically focused sheathed flow to reduce the probe volume (11 pL). At the detection limit, the probability of R-6G molecules being in the probe volume is about 0.6. In an attempt to minimize solvent fluorescence and Raman scatter, Kirsch et al. (Winefordner's group at the University of Florida) were able to detect 8,000 R-6G molecules with a relatively simple and highly sensitive laser fluorometric system where the R-6G molecules were adsorbed onto the surface of small silica spheres (10-μm diameter) and viewed individually with a fluorescence microscope.[8] Meanwhile improvements were made in the light collection efficiency of the flow cytometer, which permitted a detection limit equivalent to 125-150 fluorophores.[9] Mathies et al. (University of California, Berkeley) pointed out that the photodestruction yield is a limiting factor in attaining ultimate sensitivity with a maximum signal-to-noise ratio.[10] They were able to detect an emission spectrum arising from 3 molecules of B-phycoerythrin (B-PE), a large molecule containing the equivalent of 25 R-6G chromophores, in a probe volume of 10 pL. The

fluorescence signal from 3 B-PE molecules is several times that of the solvent background and clearly resolved from the water Raman band. These results indicated that B-PE is a very promising label for single molecule fluorescence detection. By using the LIF in hydrodynamically focused flow, Nguyen et al. (Keller's group) was able to indirectly verify the detection of single B-PE molecules as each molecule transited a focused laser beam with 180 μs transit time.[11] With similar instrumentation, Nguyen et al. (Keller's group) demonstrated a detection limit of 800 R-6G molecules in the 0.6 pL probe volume during a 1 second counting interval.[12] Peck et al. (Stanford University) observed non-random features in the autocorrelation of the signal collected with the passage of single B-PE molecules and indicated that they had achieved a detection efficiency of 15%.[13] The autocorrelation function reveals single molecule events and provides a criterion for optimizing experimental parameters. Based on the fluorescence detection of single molecule, Jett et al. (Keller's group) initiated an approach for high speed DNA sequencing.[14] The projected rate of sequencing is several hundred bases per second which is orders of magnitude faster than existing methods. With the improved sensitivity for cw laser experiments, Hahn et al. (Keller's group) have demonstrated the fluorescence detection of R-6G in aqueous solutions down to 10^{-15} M with a detection limit of 6×10^{-15} M.[15] The calibration curve was observed to be linear over 4 orders of magnitude and could be extended to higher concentrations. Single molecules of R-6G had a transit time of 1.8 ms through the 11 pL probe volume. Analysis of the data indicated that the signal-to-noise ratio for detection

of a single molecule of R-6G is 1. Using a new approach in which a rapidly pulsed laser and time-gated detection to discriminate against the Raman and other prompt scatter from the solvent and optics, Shera et al [16] (Keller's group) and Soper et al [17] (Keller s group) were able to demonstrate directly the efficient detection and counting of single chromophore molecules in aqueous solution. They had developed a technique that can efficiently distinguish between two dye molecules on the basis of differences in their emission spectra. They also demonstrated that fluorescence lifetime can be accurately determined at the single-molecule level. Wilkerson et al [18] (Keller's group) reported the first measurements of single rhodamine 110 molecule fluorescence lifetimes in a flowing, aqueous sample stream. Time-correlated single-photon counting, used in combination with mode-locked picosecond pulsed excitation, allows the detection of single fluorescent molecules in the presence of significant solvent Raman and Rayleigh backgrounds. The fluorescence lifetime of a detected molecule is estimated from the record of arrival times (relative to the excitation pulse) of photons detected during the molecule's passage through the 1 pL excitation volume. With near infrared (near-IR) excitation and detection to reduce the fluorescence impurity contribution to the background, Soper et al (Keller's group) have reported the first observation of the photon bursts arising from single near IR dye molecules (IR132) transiting through a focused Gaussian laser beam in solution with a high detection efficiency [19]. Near IR excitation and detection were used to reduce the fluorescent impurity contribution to the background, which time-gating and spectral filtering can not

overcome in most cases. The single molecule detection efficiency for the near-IR dye IR132 was found to be approximately 97%, a significant improvement when compared to the detection efficiency for the visible dye R-6G. The average number of photons detected per molecule for the near-IR dye was determined to be approximately 18. Recently, Tellinghuisen et al. (Keller's group) have shown that it was possible to record temporal data for individual fluorescent molecules of Rhodamine 110 dye in a stream of methanol [20]. The radiative lifetime of Rhodamine 110 in methanol is estimated to be 4.2 ± 0.2 ns.

Instead of using a sheath flow to confine the sample flow, Whitten et al.[21] (Ramsey's group at Oak Ridge National Laboratory) used the laser-excited fluorescence from electrodynamically levitated microdroplets to detect small numbers of R-6G molecules. The small sample volume, typically a few picoliters, reduces the background due to Raman and fluorescence emission from solvent and impurities. With 514.5-nm excitation from an argon ion laser, as few as 12 molecules have been detected in glycerol-water droplets with a signal-to-noise ratio of 3 for a single molecule of R-6G contained in a 1-pL volume (droplet diameter of 12 μm). Ng et al. (Ramsey's group) have presented experimental results demonstrating the detection of single B-PE molecules in the levitated microdroplet. Single B-PE molecules are detected with a signal-to-noise ratio greater than 4.[22]

With a very simple capillary based experimental system, Johnson et al.[23] (Winefordner's group) used a diode laser to induce fluorescence of near-IR dyes (IR140) in a flowing stream. The linear dynamic range was 6 orders of magnitude

The best limit of detection, 46 000 molecules, was achieved with a liquid jet. With some simple improvements on the above system, Lehotay et al [24] (Winefordner's group) attained a detection limit of 3000 IR140 molecules in a 250 pL probe volume. Using a metal vapor filter to absorb the laser specular scatter, Lehotay (Winefordner's group) had approached single molecule detection with a limit of detection of 800 IR140 molecules flowing in a capillary.[25] Through the experimental modifications, Lee et al. (Winefordner's group) has been able to improve the detection limit to the single molecule level.[26,27]

Applications

There are numerous potential analytical applications for single molecule detection, including DNA sequencing,[28,29] flow cytometry,[30] immunoassay, and miniaturized chemical separation techniques involving capillary electrophoresis, open tubular capillary liquid chromatography, and packed capillary liquid chromatography. An increase in the sensitivity of fluorescence detection to single molecule level will have a significant impact on many fields.

DNA Sequencing

A worldwide effort is now in progress with the ultimate goal of determining the entire nucleotide base sequence of the human genome. The magnitude of this task is apparent when one considers that there are 3×10^9 bases in the human genome. Standard procedures using electrophoresis for the separation and

identification of the DNA bases are slow and labor intensive. With the current state-of-the-art techniques, where the sequencing rate is 50,000 DNA bases per day, it will take at least 160 years to sequence the entire humane genome. The problem is much larger because the humane genome will need to be sequenced many times to determine variabilities among individual DNA bases.

Using a completely different approach, the ability to detect single fluorescent molecules in a flowing sample stream may lead eventually to a clinical instrument capable of sequencing large fragments of DNA rapidly for diagnosis of genetic diseases. This approach will involve: (1) labeling the nuclectides with base specific tags suitable for fluorescence detection, (2) selecting a desired fragment of DNA, (3) suspending the single DNA fragment in a flowing sample stream, (4) sequentially cleaving labeled bases from the free end of the DNA fragment using a cutting enzyme, and (5) detecting and identifying the cleaved, labeled bases as they flow through a focused laser beam. If the task of single molecule detection is successful (for example 1 fluorescent molecule per 1-ms transit time), the rate for DNA sequencing will be at least 1000 times faster than the current techniques.

Fluoroimmunoassay for Ligand-Receptor Interactions

The ability to detect a single molecule would revolutionize many aspects of biomedical applications, particularly immunological methods. In recent years, developments in laser based fluoroimmunoassay techniques have been limited by either the number of receptor sites, steric hindrance from the antibody, or non-

specific interactions between antibody and antigen. Therefore, it is important to develop a separation-free fluoroimmunoassay that combines the specificity of ligand/receptor interactions with the sensitivity of single molecule detection to provide an analytical technique with the potential of detecting a single specie ranging from chemical reagents to pathogens. The sensitivity of the fluoroimmunoassay will be increased if the individual fluorochrome can replace relatively large tags, such as fluorescent spheres. The ligand is labelled with the green-fluorochrome (donor) and the receptor is labelled with the red-fluorochrome (acceptor). The acceptor will generate fluorescence on the receptor only when the ligand binds to the receptor. Electronic excitation energy can be transferred from a donor to a suitable acceptor provided that the emission spectrum of the donor overlaps the absorption spectrum of the acceptor. Such a transfer can occur over distance of 1 to 10 nm. The rate of energy transfer depends on the inverse sixth power of the separation between the donor and the acceptor. In very dilute solutions, the majority of unbound ligands are too far from the receptor to enable the transfer of energy. Therefore, bound ligands activate fluorescence but free ligands do not, obviating the need for any of the traditional tedious separation procedures. Many potential donor/acceptor combinations are possible for use in the visible and near-IR. Since ligand/receptor interactions are sensitive to their microenvironment, time-resolved and polarization techniques are able to discriminate background emission from the fluorescence signal. In summary, a fluorescent excitation transfer immunoassay with the ability to detect a single

molecule would significantly contribute to the human genome program and clinical genetic analysis,

Sensitive Cellular Measurement

In some cases cell labeling and analysis is limited by the number of receptor sites or by steric hindrance from the antibodies used in present tagging procedures [21] A method with the ability to detect single (or a few) chromophores would provide more information about the structure, function, and health of cells such as DNA/RNA content, membrane potential, pH value, calcium concentration, energy transfer process, and solvent polarity

General Molecule Detection

The specificity of antibody-antigen interactions is being combined with the sensitivity of fluorescence detection to provide analytical techniques with a potential for detecting species ranging from chemical agents and hazardous molecules to pathogens The sensitivity of the antibody/antigen techniques will be increased if individual chromophores can replace the relatively large tags used For example, phycoerythrin is 1,000 times smaller than the 0 1-μm fluorescent microspheres currently used. In addition, multiple color tagging and interrogation could lead to schemes with sensitivity perhaps below the 10^{-15} M level

High-Performance Liquid Chromatography

High-Performance Liquid Chromatography (HPLC)[32] and flow injection analysis[33] have become important tools in analytical and separation chemistry. Current sensitivity and selectivity are limited by fluorescence probe volumes at the exit of the column. Typical probe volumes for HPLC are 8-10 μL, while probe volumes as small as 50×10^{-15} liter have been reported for focused flow techniques.[34] If single molecule can be detected and identified, the mating of high-performance liquid chromatography and flow injection analysis with small probe volume may make a significant contribution to clinical analysis.[35,36]

Cellular Autofluorescence Discrimination

In flow cytometry, the limit in the number of molecules that can be detected on a cell is not sensitivity but interference from autofluorescence. Although several techniques have been developed for distinguishing fluorescence associated with the tags from autofluorescence, excitation and/or detection in near-IR will benefit from the reduction in background noise sources.[37,38]

Intent of Dissertation

In this work, the emphasis is placed on the reliable measurement of a single molecule in a capillary. A major advantage of this approach is that the capillary will facilitate the analysis of extremely small volumes of solution. Furthermore, the extremely small physical dimensions encountered in a capillary column also require

detection be performed on-column, which excludes the utilization of sheathed flow cells and other types of external flow cells.

In addition, the use of e near-IR laser as e LIF excitation source is attractive since absorption is negligible for almost every type of matter, such as flow cell material, solvent, and most impurities. This is advantageous because background fluorescence from these materials does not imposa limitations on achieving e low detection limit.

However, studies at the single molecule level using an ultramicro quartz capillary tube for sample confinement have not been done, in large part because of the difficulty in discriminating against the high level of laser specular scatter caused by the capillary. Rejection of laser specular scatter has been one of the most important considerations for ultratrace analysis using LIF. An ideal optical filter for laser specular scatter would have to show nearly full absorption at the input laser wavelength while maintaining transparency over the luminescence band. The metal vapor filter (MVF) is e promising optical filter for rejecting narrow-band laser specular scatter based on the resonance absorption of an atomic vapor. The MVF is simply e heated quartz cell with parallel windows containing an inert gas and a volatile metal with e resonance atomic absorption line at the input laser wavelength. This MVF, depending on its composition, is heated to an appropriate temperature in order to produce e sufficient number density of metal atoms to absorb efficiently all detectable laser specular scatter. Therefore, the metal atoms in the MVF provide e nearly perfect optical filter for laser specular scatter as long

as the laser can be tuned to the metal vapor absorption peak and the laser linewidth is narrower than the absorption bandwidth of the MVF. Compared with conventional laser line rejection filters, such as a monochromator and notch filter, MVFs offer such advantages as low cost, high absorbance, large signal collection solid angle, narrow absorption bandwidth, and high signal throughput. Recently, several MVFs have been demonstrated to be effective in eliminating laser specular scattering for Raman spectroscopy.[39,40]

The significance of this work is in the development of a novel LIF spectroscopic technique to reliably detect a single near-IR molecule (IR140) flowing through a small probe volume (1.05 pL) within a capillary. The laser is tuned to the rubidium atomic transition line at 780.023 nm and focused onto the uncoated part of a capillary. A heated rubidium (Rb) metal vapor filter absorbs the laser specular scatter while passing the molecular fluorescence. The excitation source is a Ti:sapphire ring laser with a linewidth narrower than the rubidium atomic absorption bandwidth. The detector is a single photon avalanche photodiode with high photon detection efficiency and low dark count rate. Because of the importance of the metal vapor filter, the characteristic of the Rb MVF is evaluated theoretically and experimentally. The events coming from the arrival of single molecules are described by a statistical model based on the Poisson distribution. A weighted quadratic filter is applied to extract the photon bursts from individual single molecules as they pass through the laser beam. Detection of a single molecule in a capillary with high measurement efficiency is demonstrated.

CHAPTER 2
CONCEPT OF SINGLE MOLECULE DETECTION

Introduction

The ability to detect single molecules is largely governed by the signal-to-noise ratio (S/N) of the measurement. Kaiser has developed a statistical approach for the detection limit, which is defined as the concentration or amount of an analyte that gives a S/N of k, where k is the statistical confidence level [41] The limit of detection (LOD, k=3) corresponds to an S/N = 3, the limit of guarantee of purity (LOG, k=6) to an S/N = 6 The reciprocal of S/N times 100 is the percentage relative standard deviation (%RSD) of the measurement. Figure 2-1 shows the Gaussian probability distributions of signal due to blank (X_b), and analyte (X_s at LOD, $X_s = 3\sigma_b + X_b$, X_s at LOG, $X_s = 6\sigma_b + X_b$) [42,43] It is assumed that the noise (σ_b) is the same on the blank and on the analyte measurements near the detection limit. The limit of detection X_c is associated with an α - chance of false positive detection (mistaking a blank measurement for the analyte) The analyte is present at a concentration or amount that gives a signal at the limit of guaranteed detection X_d that is associated with a β - chance of giving rise to a measurement below X_c (false negative, mistaking the presence of analyte for the blank) Thus these two approaches to detection limit (LOD and LOG) are a figure

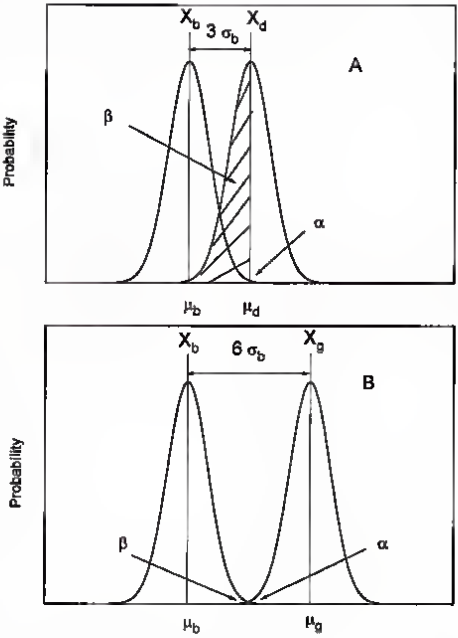

Figure 2-1 Concept of LOD (A) and LOG (B)

of merit that describe the detection power of an analytical method. In practical applications, the value of detection limit indicates the level of analyte that might be discerned from the background noise. If measured carefully, the LOD and LOQ can give an objective comparison of the detection power of different analytical methods. The LOD has a low probability of false positives (α, type I error), 0.14%, but a high probability of false negatives (β, type II error), 50%. The LOQ is a more conservative analytical figure of merit which has very low probability of a false positives (α, type I error), below 0.14%, and a low probability of a false negatives (β, type II error), about 0.14%. This means that when the analyte is present in the sample at the LOD value, fully 50% of the measurement will fall below X_d even though there is only a 0.14% probability that the measurement of a blank will give a false positive. On the other hand, if the analyte is present at the LOQ value, measurement on the sample will be always detected above X_d at the 99.86% confidence level.

The first theoretical treatment for the concept of detection limit that applicable to single molecule detection was developed by Alkemade [44,45]. In terms of intrinsic and extrinsic detection limits, Winefordner et al.[44,45] and Stevenson et al.[46,47,48] have shown theoretically that laser-induced fluorescence (LIF) is the only viable approach for single molecule detection. Methods which have achieved single molecule detection using LIF are usually based on a "cyclic" interaction of molecule and laser, and each molecule produces a relatively large number of photons during its interaction with the laser (see Chapter 1 laser-induced

fluorescence photon burst detection). An ideal technique for single molecule detection will meet the following demands simultaneously.

(i) the efficiency of detection, ϵ_{in}, and the efficiency of measurement, ϵ_{out}, are both unity

(ii) intrinsic noise dominates extrinsic noise

Detection Efficiency

Alkemade defined the detection efficiency as the probability that any given species appearing in the probe volume produces an event during the transit time.[44,45] The probe volume was determined by the geometry of the (intersecting) laser beam and by the part of the irradiated region that is "seen" by the detector. In the Alkemade approach, the transit time was determined by the pulse duration or the width of the time gate in case a time-gating circuit is applied, whichever is the shorter. Multiple probings are obtained by firing many laser shots. In addition, Alkemade was concerned only with those cases when there were no extrinsic noise sources.

Winefordner et al.[42,43] and Stevenson et al.[40,47,48] have developed a theory to take into account the transit time of a single molecule within the probe volume and the presence of extrinsic noise sources. When compared with Alkemade's concepts, Winefordner's are more general in two important aspects.

(1)detection efficiency is defined with respect to a transit time of the molecules in the probe volume, not simply over a single "probing" of the

laser pulse.

(2)detection efficiency considers the need to detect the signal due to analytes over the extrinsic noise

Therefore, the detection efficiency is defined as the probability that a given analyte appearing in the probe volume produces a signal that is detected above the background noise (if any) during the transit time of the analytes within the observation region

The general definition of the detection efficiency, ϵ_{det} is determined by the interaction of single molecules with the laser during the measurement time, T_m :

$$\epsilon_{det} = P\left(X_t \geq X_d \right) \qquad (2\text{-}1)$$

where $P(X_t \geq X_d)$ is the probability that the analyte measured is greater than the detection limit measured, predefined for false positives. The term X_d is the number of signal counts at the detection limit and X_t is the number of signal counts produced by a molecule during the measurement time T_m. Assuming there is a Poisson detection process, the probability of a single molecule producing the single molecule events is given by

$$P\left(X_t \geq X_d\right) = 1 - e^{-\phi_s \Delta t} \qquad (2\text{-}2)$$

where ϕ_s is the mean flux of signal from a given molecule (counts s^{-1} molecule^{-1}), and Δt is the interaction time (transit time) of each molecule within the laser beam. Note that the measured sensitivity, X_t-X_b, is equal to $\phi_s \Delta t$ in equation (2-2). For

a LIF method, ϕ_s is the rate (s^{-1}) of detected events from a single molecule. The general definition of single molecule detection is that the method detects each and every molecule that interacts with the laser. Therefore

$$\epsilon_d \geq 1 - \beta \qquad (2\text{-}3)$$

where β is the probability of the false negatives (type II error).

The detection limit can be used to define the requirement for achieving single molecule detection with LIF.

$$X_f \geq X_d - X_b \qquad (2\text{-}4)$$

where X_b is the mean background flux. Table 2-1 gives the measurement sensitivity, X_d, required to detect single molecules using LIF at various mean blank signal levels (α=0.0014 for LOD and β=0.0014 for LOQ). For example, at the intrinsic noise limit (X_b=0), a value of X_f=1 count molecule^{-1} and X_f=6.6 counts molecule^{-1} is needed to detect a single molecule event for LOD and LOQ, respectively. This means that, in order to detect every molecule that crosses the laser with 99.86% confidence (LOQ), then each molecule must emit enough photons so that, on average, 6.6 counts are registered for the molecule by the detector. As the background level increases, eg., to 1 count, the number of analyte counts from a single molecule above the blank increases to 5 counts molecule^{-1} (total 5+1 counts molecule^{-1}) at LOD and 15 counts molecule^{-1} (total 15+1 counts molecule^{-1}) at LOQ.

Table 2-1 The two detection limits for an single molecule detection experiment.

Mean blank, X_b (counts)	Mean sensitivity, X_L (counts)	
	LOD=1 molecule $\alpha \leq 0.0014$	LOG=1 molecule $\beta = 0.0014$
0.00	1	6.6
0.05	2	6.9
0.25	4	12.4
1.00	5	15
5.00	9	23
10.00	12	29
100.00	32	69

Measurement Efficiency

The overall measurement efficiency, ϵ_m, is defined as the probability that a given analyte in the sample is detected above the background noise in the observation region. The measurement efficiency, ϵ_m, is related to the detection efficiency, ϵ_d, by the following equations:

$$\epsilon_m = \epsilon_T \epsilon_P \epsilon_d \qquad (2\text{-}5)$$

$$\epsilon_P = \epsilon_s \epsilon_t \qquad (2\text{-}6)$$

where ϵ_T is the transfer efficiency of the sample from the point of introduction to the probing region and ϵ_P is the probing efficiency which is composed of a spatial probing efficiency, ϵ_s, and a temporal probing efficiency, ϵ_t (see equation (2-6)). The spatial probing efficiency, ϵ_s, accounts for the loss of analyte species without passing the laser excitation and/or observation region. The temporal probing efficiency, ϵ_t, is unity for a cw source or a pulsed source which is at a repetition rate sufficiently high such that each analyte species interacts with at least one laser pulse while passing through the observation region. Unlike ϵ_d, the value of ϵ_m is related to analyte concentration in the sample and may be less than unity even if ϵ_d = 100% since ϵ_m accounts for analyte losses between the sample and the detection region and for insufficient spatial and temporal probing of analytes as they appear within the probe volume.

Even if single molecule detection with high detection efficiency has been

achieved in the sheathed flow cell, the measurement efficiency may be far less than unity. In the approach using the sheathed flow cell, the hydrodynamic focusing sample stream is flowing through a square sheathed flow cell to minimize the laser specular scatter caused by the optical materials.[7,11,12,14] Furthermore, as shown in Figure 2-2, the laser beam only probes a small portion of sample stream to reduce the Raman and background scatter from the solvent and the optical materials. A spatial filter (slit) placed before the detector only images a small region of probe volume to reduce the amount of laser scatter generated at the air-glass interface. Therefore, the spatial probing efficiency for single molecule detection in a sheathed flow cell is only 0.01% which means approximately 0.01% of those molecules that pass through the flow cell are detected even if detection efficiency is unity (ϵ_d=1.00). This single molecule detection with low measurement efficiency (due to low spatial probing efficiency) is not appropriate for such applications as DNA sequencing where detection of every DNA base is essential.

When compared with the sheathed flow cell method, this work uses the laser beam to illuminate the whole sample stream which is confined in a capillary as shown in Figure 2-3. Therefore, every molecule passed through the capillary flow cell should be detected with near unity measurement efficiency (ϵ_m).

Estimation of Detection Limit

For LIF detection, the number of detected photoelectrons, N_e, is given by

$$N_e = Y N_m \qquad (2\text{-}7)$$

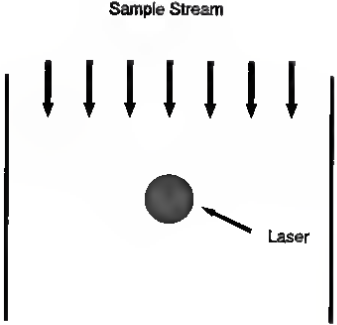

Figure 2-2 Single molecule detection in sheathed flow cell

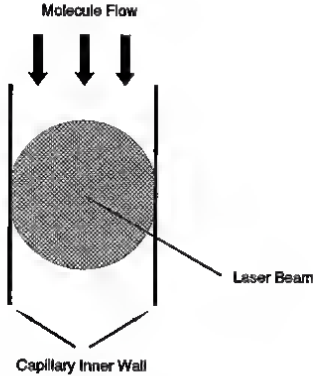

Figure 2-3 Single molecule detection in capillary flow cell

where N_e is the number of detected photoelectron counts during the transit time, Y is the measurement sensitivity, in photoelectron counts/molecule, and N_m is the number of molecules detected in the sample during the transit time in the probe volume. The measurement sensitivity Y is given by

$$Y = \phi_e \, \Delta t_t \, \epsilon_T \, \epsilon_D \tag{2-8}$$

where ϕ_e is the mean flux of detected events, in photoelectron counts/sec and Δt_t is the transit of molecule within the probe volume. The ϕ_e is a function of emission transition probability (A), fluorescence collection efficiency (η_c), and detector quantum efficiency (η_d).

To be detected, the molecules must produce a large enough signal, N_e, so that

$$N_e \geq X_d - X_b \tag{2-9}$$

where X_d is total signal counts (including analyte and background) at detection limit and X_b is the mean background flux during the transit time for the single molecules passing through the probe volume. Note that the value N_e is equal to the number of signal counts from a single molecule in the second (LOD) and/or third columns (LOQ) of Table 2-1. Therefore, the detection limit for molecules in the laser excited region is given by

$$N_{DL} = \frac{X_d - X_b}{Y} \tag{2-10}$$

where X_a is the total number of counts from background and analyte. Thus if X_a-X_b is 6.6 counts (definition of LOG), the measurement sensitivity Y must be at least 6.6 counts to assure a guaranteed limit of one single molecule

Formal Description of LIF in Capillary

In order to obtain the highest signal counts in LIF photon burst detection, the photoexcitation rate must be maximized while the photodestruction rate of molecules must be minimized.[49] The photon absorption rate k_a (photons sec^{-1} $molecule^{-1}$) by a chromophore having an absorption cross section σ_a (cm^2/molecule) illuminated by an incident beam of intensity I (photons/cm^2 sec) is given by

$$k_a = \sigma_a I \qquad (2\text{-}11)$$

The equation (2-11) is valid when the ratio of excitation is small compared with the excited state decay rate $1/\tau$, where τ is the excited state lifetime of the chromophore. The absorption cross section is related to the molar absorbance coefficient ϵ ($cm^{-1}M^{-1}$) by

$$\sigma_a = 3.8 \times 10^{-21} \epsilon \qquad (2\text{-}12)$$

For a Gaussian beam with a radius ω (where the intensity is $1/e^2$ of its peak value) and power P (photons/sec), the mean intensity I is equal to $P/(\pi\omega^2)$, and so

$$k_a = 3.8 \times 10^{21} \epsilon \frac{P}{\pi \omega^2} \qquad (2\text{-}13)$$

Assuming a nonsaturating excitation condition, the rate of fluorescence emission k_f (photons/sec) is the product of k_a and the fluorescence quantum yield Q_f. Hence,

$$k_f = \sigma_a I Q_f = 3.8 \times 10^{21} \epsilon Q_f \frac{P}{\pi \omega^2} \qquad (2\text{-}14)$$

The fluorescence rate of the molecules can be calculated using equation (2-14). For example, IR140 has an absorption coefficient $\epsilon = 2.1 \times 10^5$ $cm^{-1}M^{-1}$ at an excitation wavelength of 780.023 nm. If a 10 mW laser is used as the excitation source focused to a beam diameter of 11 μm, the excitation power is 3.9×10^{15} photons/sec. In the case of $Q_f = 1$, the fluorescence emission rate is 8×10^5 photons/sec.

In practice, photodestruction processes limit the number of times that a given molecule can be cycled through the excitation process. When LIF detection is optimized to achieve ultimate sensitivity, a more detailed expression than equation (2-14) is needed to estimate the rate of fluorescence. During high light intensity conditions, both ground-state depletion, which is caused by pumping a significant fraction of the molecules to their excited state, as well as photodestruction from the excitation state must be taken into account. As an

approximation, the average number of photons n_f that a fluorescent molecule can yield is given by [49,50]

$$n_f = \frac{Q_f}{Q_d} \tag{2-15}$$

where Q_d is the photodestruction quantum yield. This simple result shows that the maximum number of photons that can be obtained from a fluorescent molecule is equal to the fluorescence quantum yield divided by the photodestruction quantum yield. This expression makes intuitive sense since the maximum number of fluorescent photons is necessarily related to the branching ratio for the two processes (i.e., fluorescence and photodestruction) that remove population from the excited state.

Unfortunately, when the laser intensity is increased the signal-to-noise (S/N) ratio will start to level off. This is due to the fact that the rate of photodestruction and the rate of fluorescence are not linearly dependent on the incident laser power at high intensity conditions. Furthermore, the decrease in the S/N ratio is also due to the fact that background scattering is linearly dependent on laser intensity. Therefore, the S/N ratio will decrease once fluorescence saturation or photodestruction occurs. Mathies et al.[48] have presented a thorough treatment of high sensitivity LIF detection in which the following equations can be used for a detailed theoretical optimization.

$$n_f = \frac{Q_f}{Q_d}\left[1 - e^{-\frac{k\tau}{k\tau - 1}}\right] \qquad (2\text{-}16)$$

and

$$k = \frac{k_a}{k_f^0} \qquad (2\text{-}17)$$

$$\tau = \frac{\tau_t}{\tau_d} \qquad (2\text{-}18)$$

where k_a is rate of absorption, k_f^0 is observed rate of fluorescence τ_t is transit time, and τ_d photodestruction time It is clear from this treatment that the photodestruction quantum yield ϕ is an important figure of merit in evaluating new fluorescent labeling dyes and improving high-sensitivity fluorescence detection methods

Since photodestruction is a critical parameter in optimizing S/N ratio for high sensitivity LIF detection, knowledge of photodestruction quantum yield ϕ is essential. A simple approach for measuring the photodestruction quantum yield has been devised by Mathies et al [51] and White et al [52] In this approach, the fluorescence intensity of the dye solution is measured as a function of the flow rate of dye passing through a capillary tube placed at the focus of the pump laser beam The dependence of the fluorescence intensity on the flow rate is related to

a key parameter, the photoelteration coefficient, F, which is given by

$$F = \frac{3.8 \times 10^{-21} \epsilon P Q_d}{\sqrt{\pi}\ \omega\ v} \qquad (2\text{-}19)$$

where ϵ is the molar absorbance coefficient ($cm^{-1}M^{-1}$), P is the incident laser power (photons s^{-1}), Q_d is the photodestruction quantum yield, ω is focused laser beam radius (cm), and v is the linear flow velocity (cm s^{-1}) of the dye solution passing through the probe volume excited by the laser beam. A normalized fluorescence intensity S' can be calculated such that

$$S' = \frac{1}{\pi}\int_{-\infty}^{\infty}\int_{-\infty}^{\infty}[\exp-(s^2+t^2)]\times\exp-[\sqrt{2/\pi}F\int_{-\infty}^{\infty}\exp-(s^2+t^2)ds']ds\,dt \qquad (2\text{-}20)$$

and

$$S' = \frac{S(F)}{S(0)} \qquad (2\text{-}21)$$

where S(F) is the fluorescence intensity observed at a particular value of F, S(0) is the fluorescence intensity that would be observed if the dye molecule were not photolable, s is the relative position at flow axis, and t is the relative position at detection axis

Unfortunately, the use of equation (2-20) for numerical calculations requires high computational capacity because of its complexity. The equation is, therefore,

rewritten to a more useful form that is easy to implement on a personal computer,[30]

$$S' = \frac{1}{F}\sqrt{\frac{2}{\pi}} \times \int_0^1 \frac{1 - \exp -(\sqrt{2}\, F\, u)}{2\, u \sqrt{-\log u}}\, du \qquad (2\text{-}22)$$

where u is an integration variable. Measuring S' as a function of the flow velocity will then reveal the photodestruction quantum yield Q_d from equation (2-19) to equation (2-22).

The above equations have been used to evaluate the photodestruction quantum yield Q_d for fluorescein and B-phycoerythrin.[18] The experimental parameters for both visible dye molecules is given in Table 2-2. The simulated photodestruction curves using equation (2-22) are shown in Figure 2-4 and Figure 2-5 for fluorescein and B-phycoerythrin, respectively.

Noise Sources

Noise in a measurement can be classified as either extrinsic or intrinsic. Extrinsic noise is the excess noise which arises owing to a nonspecific background signal that is present even in the absence of analyte. Extrinsic noise sources are determined by such instrumental factors as dark current, source light scatter, a background emission from concomitants, and nonselective detection of molecules in blank. Intrinsic noise represents the ultimate limit of an analytical method and is determined by the statistical nature of the measurement process, such as the discrete nature of matter, fluctuations in the low number of analytes in the probe

Table 2-2 Experimental parameters for fluorescein and B-phycoerythrin.

	Fluorescein	B-Phycoerythrin
Molar absorption coefficient	8.0×10^4 cm^{-1}M^{-1}	1.4×10^6 cm^{-1}M^{-1}
Laser power	2.2×10^{17} photons/s	3.9×10^{16} photons/s
Photodestruction quantum yield	2.7×10^{-5}	1.1×10^{-6}
Beam radius	4 μm	18 μm

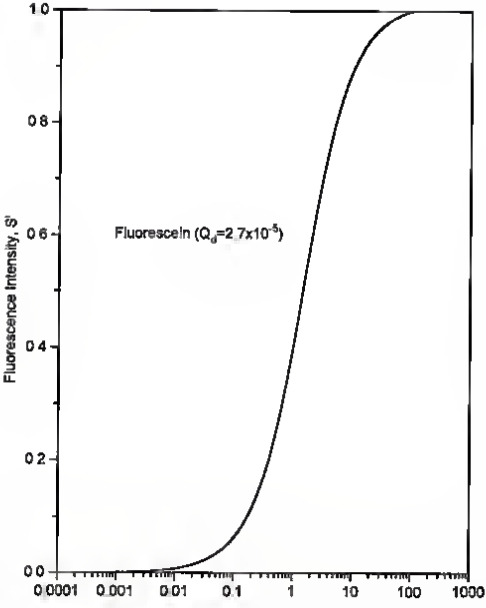

Figure 2-4 The simulated photodestruction curve for fluorescein

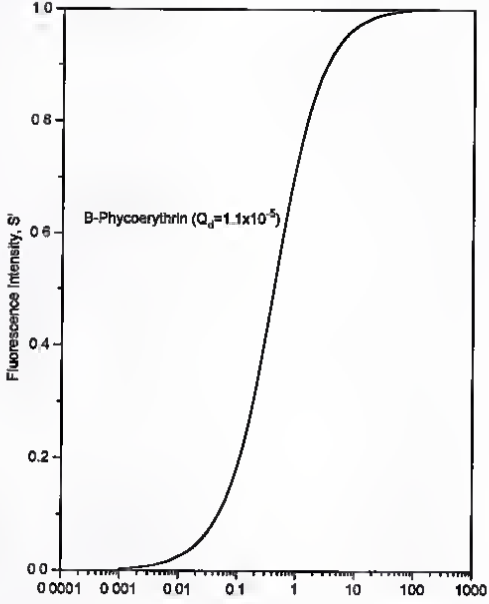

Figure 2-5 The simulated photodestruction curve of B-Phycoerythrin.

volume, and shot noise in analyte signal production. As intrinsic noise arises from the detection of analytes, it can not be removed. In this work, by reducing all sources of background noise, i.e., by excitation in the near-IR, by use of a metal vapor filter, by use of an appropriate spectral filter, by optimizing the laser characteristics, intrinsic noise should dominate the extrinsic noise for single molecule measurement.

In a counting measurement, it is possible to reduce all extrinsic noise sources to the extent that the probability of registering one or more counts from the blank is negligible during the transit time. For such an intrinsic-noise limit measurement, the only noise on the signal is due to the statistical nature of the analyte detection process itself. Signal noise in an extrinsic-noise limited experiment is due to contributions from both extrinsic and intrinsic noise sources.

In order to reach the intrinsic noise detection limit, all the extrinsic noise sources must be minimized. In a typical LIF experiment, there are three major limiting sources of extrinsic noise -- laser specular scatter, Raman scatter, and background fluorescence.

In nearly every laser-induced fluorescence analysis, laser specular scatter constitutes the most severe source of noise. In this work, the laser scatter problem becomes worse when the laser beam is focused onto a capillary with a small diameter. For example, the number of photons delivered by the 10 mW laser at 780.023 nm is approximately 4×10^{16} photons/sec. Assume only 0.1% of photons reflected from the capillary wall is collected and reach the detector. This

still corresponds to at least 10^{10} photons per transit time (in this work, molecular transit time = 1 ms) which is several orders of magnitude higher than the maximum number of photons emitted from a single molecule (10 - 1000 photons/transit time). Several types of optical filters, such as a monochromator, polarizer, spectral band pass filter, and spatial filter, have been applied to minimize the intense laser specular scatter. Unfortunately, all the optical filters above have drawbacks such as low optical density, low spectral band pass, incident angle sensitivity, and difficulty of use (to be discussed in Chapter 3). Therefore, the development of a new optical filters with high absorbance and large spectral band pass is essential for single molecule detection. The metal vapor filter is a promising optical filter that can be applied to absorb the intense laser specular scatter while maintaining high signal transmittance. According to absorption theory (to be discussed in Chapter 3), the metal vapor filter is capable of totally absorbing the laser specular scatter provided the laser linewidth is narrower than the absorption bandwidth of metal vapor filter. Moreover the metal vapor filter only removes the laser radiation at a specific wavelength but does not hinder the transmittance of the entire fluorescence emission band. Because of its role in absorbing the laser specular scatter from the collected signal, the metal vapor filter is one of the most important experimental components to attain single molecule detection.

Unlike laser specular scatter, Raman scatter is an inelastic process that occurs typically with a cross-section of 10^{-30} cm^2 per molecule [3]. The large amount of Raman scatter from solvent or impurities produces background photons that

can be significantly greater in number than the fluorescence photons from single molecules. In typical laser-induced fluorescence detection, noises due to Raman scatter from the solvent or impurities become the limiting source of noise when the laser specular scatter is reduced. Lehotay has measured the Raman scatter of methanol at approximately 960 nm when excited at 780.023 nm.[35] To decrease the number of solvent or impurity molecules, reducing the probe volume has been the other approach to minimize the Raman scatter. In this work, the uses of a very small probe volume (1.05 pL) and a spectral band pass filter are applied to optimize the S/N ratio for single molecule detection.

Because of the large absorption cross section (approximately 10^{-16} cm^2 per molecule) of analytes in visible radiation, several approaches for single molecule detection utilizing argon ion laser have suffered significant noise problems from the background fluorescence of optical material, solvent, and impurities.[53] To overcome this problem, near-IR fluorescence detection has been suggested as a viable alternative to visible fluorescence detection due to limited number of compounds that demonstrate intrinsic fluorescence in the near-IR.[54,55,56,57,58,59,60] In fact, the only known molecules to fluoresce strongly in the near-IR are the cyanine dyes known as polymethines (to be discussed in Chapter 5).[61] When compared with the more commonly used 514.5 nm line from an argon ion laser, an additional advantage of using near-IR excitation is that the Raman scatter process is reduced by a factor of 1/(excitation wavelength)^4, and background fluorescence is also reduced. Therefore, the use of near-IR as the excitation source will benefit single

molecule detection because of the substantial reduction in background noise sources.

CHAPTER 3
METAL VAPOR FILTER

Introduction

Rejection of laser specular scatter is the most important consideration for ultratrace analysis using laser-induced fluorescence. Indralingam et al. have reviewed the use of various optical filters for laser scatter rejection.[30] Different types of optical filters possess some disadvantages in terms of light rejection power, signal throughput, and the ease of use. A monochromator has a very high light rejection power typically on the order of 10^5. Unfortunately, the spectral bandpass and the signal throughput are also greatly reduced which lowers the signal as well as the laser scatter. Therefore, the application of monochromator is inadequate. A spectral filter is a common approach in reducing laser scatter in LIF experiments. The light rejection capability of band-pass spectral filters, long-pass spectral filters, and short pass spectral filters is approximately 10^3, which is poorer than most monochromators, but these spectral filters generally have a much greater optical throughput of the fluorescence signal. Usually, two or more spectral filters are used together or in conjunction with a monochromator. The problem of the spectral filter is the low light rejection power. Polarized filters are another approach to reduce the laser scatter due to different polarities of the

fluorescence and the scattered radiations. Ideally, polarized filters are capable of 10^9 rejection of light polarized 90° to the transmitted light. In practice, polarized light rejection does not work as well as expected due to the lack of purity of the laser scatter polarity. The concept of spatial filtering has been successfully applied to ultratrace analysis for S/N ratio improvement.[52] With careful positioning and focusing, a slit or pinhole can pass a large portion of the fluorescence signal while blocking much of the laser scatter arising from the edge of the sample confinement. The problem with the spatial filter is that it can limit the probe volume of the measurement by collecting fluorescence emission from only a portion of the focused region. Although the S/N ratio can be improved, the measurement efficiency is below unity. Therefore, spatial filters also are not suitable as light rejecters for single molecule detection.

The metal vapor filter is a promising optical filter for narrow band laser scatter based on the resonance absorption of an atomic vapor. Metal vapor filters offer such advantages as very high absorbance, a hemispherical field-of-view, a very narrow rejection linewidth, and high signal throughput. Table 3-1 is a list of several elements that could be of practical use in a MVFs along with their rejection wavelength and the estimate of the operation temperature required for a strong optical attenuation (absorbance > 5).[46] There has been a recent resurgence of interest in MVFs with reports of near IR Raman spectroscopy using alkali metal vapors to filter scattered laser light, probably as result of the convenience of the Ti:sapphire laser as a tunable excitation source. Indralingam et al. measured

Table 3-1 Potential atomic metal vapor filters.

ATOM	λ (nm)	T (°C)	ATOM	λ (nm)	T (°C)
Cs	894.35	73	Na	342.69	274
Cs	852.11	63	Rb	335.09	242
Rb	794.76	88	Rb	334.87	211
Rb	780.02	78	Na	330.30	281
K	769.90	121	Cd	326.11	274
K	766.49	111	Li	323.26	524
Li	670.79	411	Zn	307.59	423
Li	670.78	377	Ba	307.16	560
Na	589.59	192	Mg	285.21	288
Na	588.99	181	Tl	276.79	471
Ba	553.55	500	Li	274.12	532
Cs	459.32	125	Cs	272.16	460
Cs	455.53	125	Tl	258.01	551
Cs	422.57	406	Li	256.23	542
Rb	421.56	162	Hg	253.65	20
Rb	420.18	145	Li	247.51	557
K	404.72	209	Li	242.54	583
K	404.41	194	Ca	239.85	507
Cs	388.86	206	Tl	237.97	510
Tl	377.57	494	Tl	231.60	593
Cs	361.15	185	Cd	228.80	163
Rb	359.16	206	Ca	227.55	490
Rb	358.71	137	Tl	223.78	540
Ba	350.11	580	Zn	213.86	231

Raman scattering from transparent materials using a single stage grating spectrometer and a rubidium metal vapor filter to absorb any collected laser scatter.[39] A rubidium atom possesses a very strong ground state optical absorption at 780.02 nm and 794.76 nm, the wavelengths which can be easily accessed using a Ti:sapphire laser. Pelletier measured the 9.6 cm^{-1} anti-Stokes band of l-cystine using a double monochromator and a Ti:sapphire laser tuned to the 766.49 nm absorption line of potassium in a potassium vapor cell for near-IR laser light absorption.[40] Both groups also highlighted a major drawback involving a window discoloring problem due to atom condensation. This chapter will present a numerical evaluation of the Voigt absorption profiles for metal vapor filters which are capable of essentially totally absorbing laser scatter provided that the laser radiation linewidth is narrower than the absorption bandwidth of the metal vapor.

Operation Principle

An ideal metal vapor filter for laser scatter rejection would have to show nearly full absorption at the input laser wavelength while keeping transparency to the output signals. The metal vapor filter consists simply of a heated cell with parallel windows and contains a buffer gas, such as nitrogen at several hundred Torr, and a volatile metal, such as an alkali metal, with a resonance absorption peak at the wavelength of the laser line. The metal vapor filter, depending on its composition, will be heated to an appropriate temperature in order to produce a sufficient number density of metal atoms to absorb effectively all detectable laser

scatter. Therefore, the metal atoms in the metal vapor filter will provide a "perfect" filter for laser scatter as long as the laser radiation can be tuned to the absorption peak of the metal vapor and as long as the Gaussian laser line has a FWHM (full width at half maximum) less than the absorption bandwidth of metal vapor filter.

Line Broadening Mechanisms

To evaluate the capability of laser scatter rejection, the absorption spectral profile of a metal vapor filter must be characterized. There are various broadening mechanisms of atomic line shape.[53]

Natural Broadening

Because of interaction of atoms with radiation fields and collisional processes, the lower, i, and upper, j, energy states participating in the atomic excitation have a finite lifetime, and this gives rise to uncertainties in the energy of both states according to the Heisenberg uncertainty relation. The broadening due to the radiative lifetime is thus called natural broadening. The FWHM linewidth $\Delta\nu_N$ caused by natural broadening is

$$\Delta\nu_N = \frac{1}{2\pi\tau_r} \qquad (3\text{-}1)$$

where

τ_r = radiative lifetime

For many atoms the natural lifetime, τ_n, is on the order of 10^{-8} sec. Therefore the linewidth, $\Delta\nu_N$, of natural broadening is approximately 1.6×10^7 Hz. In wavelength units the half-intensity width, $\Delta\lambda_N$, is given by

$$\Delta\lambda_N = \frac{\Delta\nu_N \lambda_m^2}{c} \tag{3-2}$$

where

λ_m = wavelength at the line center (m)

c = speed of light (m s^{-1})

For example the $\Delta\lambda_N$ is 2×10^{-14} m or 0.02 pm for sodium, Na, at 589.0 nm. The spectral profile function of a naturally broadened line is described by a Lorentzian function. The normalized spectral profile function due to natural broadening, $S_{\nu N}$, is given by

$$S_{\nu N} = \frac{\frac{2}{(\pi\,\Delta\nu_N)}}{1 + \left[\frac{2\,(\nu_m - \nu)}{\Delta\nu_N}\right]^2} \tag{3-3}$$

where

$\Delta\nu_N$ = FWHM of the naturally broadened line (Hz)

ν_m = frequency at the line center (Hz)

For the applications in metal vapor filters, the natural linewidth is hidden beneath other broadening mechanisms and can safely be neglected.

Collisional Broadening

Collisional (or pressure) broadening is caused by the perturbation of the energy levels of an atom by collision with surrounding atoms. Collisions that leave the atom in the same energy state (adiabatic collisions) have a more pronounced broadening effect than collisions that leave the atom in a different energy state (diabatic collisions). The spectral distribution of adiabatic collisional (pressure) broadening can be described by a Lorentzian line shape with a linewidth

$$\Delta\nu_a = \sigma_c\, n_x \left[\frac{8\ k\ T}{\pi^3\ \mu}\right]^{1/2} \qquad (3\text{-}4)$$

where

σ_c = optical cross section of collisional partner (cm^2)

n_x = number density of collision partner (cm^{-3})

μ = reduced mass of collision partners (g)

The typical FWHM of a collisionally broadened line is on the order of $3x10^{-12}$ m or 3 pm. The total, normalized Lorentzian spectral profile function, $S_{\nu L}$, for collisional broadening is similar to equation (3-3) except that the natural FWHM, $\Delta\nu_n$, is replaced with the Lorentzian FWHM, $\Delta\nu_L$

$$S_{\nu L} = \frac{\dfrac{2}{(\pi\ \Delta\nu_L)}}{1 + \left[\dfrac{2\ (\nu_m - \nu)}{\Delta\nu_L}\right]^2} \qquad (3\text{-}5)$$

where

$\Delta\nu_L$ = FWHM of the collisionally broadened line (Hz)

ν_m = frequency at the line center (Hz)

If natural and collisional broadening are assumed to be mutually independent, the resulting FWHM of the Lorentzian spectral profile is the summation of the collisional spectral linewidth $\Delta\nu_C$ and the natural spectral linewidth $\Delta\nu_N$

$$\Delta\nu_L = \Delta\nu_C + \Delta\nu_N \qquad (3\text{-}6)$$

Doppler Broadening

Doppler line broadening results from the motion of absorbing atoms at different velocities relative to the source or detector. Doppler broadening is described by a Gaussian profile with FWHM given by

$$\Delta\nu_D = \frac{2\,\nu_m}{c}\left[\frac{2\,(\ln 2)\,k\,T}{m}\right]^{1/2} \qquad (3\text{-}7)$$

where

k = Boltzmann constant (JK^{-1})

m = Atomic weight (g)

ν_m = Frequency at the line center (Hz)

For atoms in flames $\Delta\lambda_D$ is typically 10^{-12} m (1 pm) to 10^{-11} m (10 pm). The normalized spectral profile function with Gaussian distribution is given by

$$S_{\nu D} = \frac{2\sqrt{\ln 2}}{\Delta\nu_D\sqrt{\pi}} \exp\left[-\frac{(\ln 2)(\nu - \nu_m)^2}{\Delta\nu_D^2}\right] \qquad (3\text{-}8)$$

where

$\Delta\nu_D$ = FWHM of the Doppler broadened line (Hz)

ν_m = frequency at the line center (Hz)

The predominance of one type of broadened profile over another is largely dependent on the environment of atoms. Figure 3-1 shows the relative absorption profiles for purely collisional (Lorentzian) and purely Doppler (Gaussian) broadened lines. These broadened line profiles are calculated using equation (3-5) and equation (3-8) respectively, with FWHM of 10 pm centered at 780.023 nm. In one case, the laser with pure Gaussian spectral profile and narrow linewidth, both collisional (Lorentzian) and Doppler (Gaussian) broadening can be used to evaluate the absorbance in the metal vapor filter applications. In the other case, if the laser has a long wing and/or pedestals that extended away from the laser line center, the performance of the metal vapor filter will be degraded since the long wing and/or pedestals can not be rejected efficiently by both broadening absorption bands (as seen in the shaded area of Figure 3-2).

Voigt Spectral Profile

Because Doppler broadening produces a Gaussian profile and pressure broadening produces a Lorentzian profile, the overall spectral line shape is a

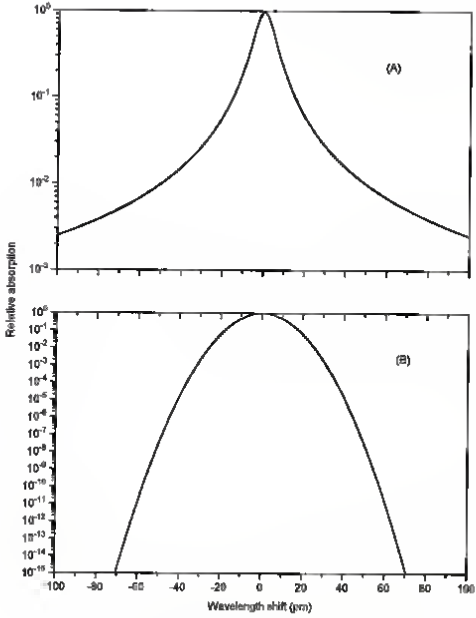

Figure 3-1 Normalized Lorentzian (A) and Gaussian (B) line profile

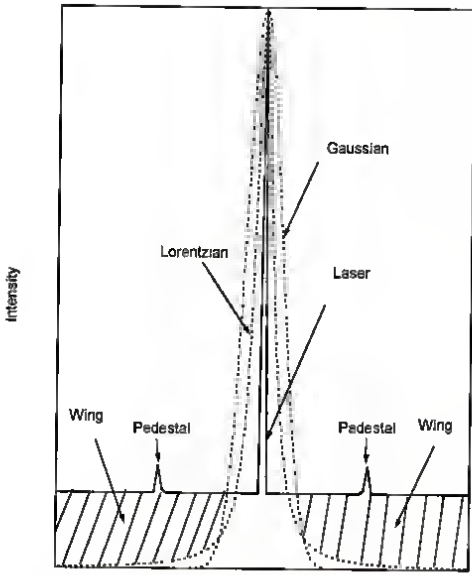

Figure 3-2 Effect of laser profile on aborbance of Rb MVF (not to scale)

convolution of Gaussian and Lorentzian functions. If line asymmetry is ignored and the two types of broadening are assumed to be independent, the convoluted spectral profile function can be described by the Voigt function with a FWHM linewidth $\Delta\nu_V$

$$\Delta\nu_V = \frac{\Delta\nu_L}{2} + \left[\left(\frac{\Delta\nu_L}{2}\right)^2 + \Delta\nu_D^2\right]^{1/2} \qquad (3\text{-}9)$$

The spectral line shape is a Voigt function, which is the convolution of a Lorentzian profile and a Gaussian profile,

$$S_{\nu V} = \frac{1}{\Delta\nu_D}\left(\frac{\ln 2}{\pi}\right)^{1/2} \int_{-\infty}^{+\infty} \frac{\exp(-\zeta^2)}{\mu^2 + (\xi - \zeta)^2}\, d\zeta \qquad (3\text{-}10)$$

where

$$\xi = \frac{\nu - \nu_m}{\Delta\nu_D}\sqrt{2\ln 2}$$

$$\mu = \frac{\Delta\nu_L}{\Delta\nu_D}\sqrt{2\ln 2}$$

and ζ is an integration variable. Unfortunately, the convolution integral describing the Voigt function (equation (3-10)) can not be evaluated analytically. Various numerical approximations and expansions of this Voigt spectral profile function have been developed by many investigators and summarized by Jansson and Korb[65]. Puerta and Martin give an excellent and reliable approximation to the Voigt

line shape by four generalized Lorentzian functions.[44,45] The form given by Puerta and Martin is

$$J(d, p) = \frac{p}{\pi} \int_{-\infty}^{+\infty} \frac{\exp(-\zeta^2)}{p^2 + (d - \zeta)^2} d\zeta \qquad (3\text{-}11)$$

and can be numerically approximated by

$$J(d,p) = \sum_{j=1}^{4} \frac{\gamma_j (p - \alpha_j) + \delta_j (d - \beta_j)}{(p - \alpha_j)^2 + (d - \beta_j)^2} \qquad (3\text{-}12)$$

where

$$d = \frac{\nu - \nu_m}{\Delta\nu_D} \sqrt{2 \ln 2}$$

$$p = \frac{\Delta\nu_L}{\Delta\nu_D} \sqrt{2 \ln 2}$$

The values of the approximation parameters α_j, β_j, γ_j, and δ_j are given in Table 3-2. When compared with the Gaussian and Lorentzian spectral profile functions, the shape of the Voigt spectral profile function has a wing broader than the Gaussian's, but not as broad as the Lorentzian's.

Absorbance of Rubidium 780.023 Line

In the case of atomic absorption, the measurement result is expressed as

Table 3-2 The value of the approximation parameters for Puerta and Martin's Voigt function.

Parameter	j=1	j=2	j=3	j=4
α_j	-1 2150	-1 3509	-1 2150	-1.3509
β_j	1 2359	0 3786	-1 2359	-0 3786
γ_j	-0 3085	0 5906	-0 3085	0.5906
δ_j	0 0210	-1 1858	-0 0210	1 1858

the absorption factor, α, or the absorbance, A, which are related to the transmittance T by

$$\alpha = 1 - T \tag{3-13}$$

$$A = -\log T \tag{3-14}$$

The transmittance **T** is given by

$$T = \frac{\Phi}{\Phi_0} \tag{3-15}$$

where Φ is the transmitted radiant power and Φ_0 is the incident radiant power. The absorption factor α is the radiant power absorbed ($\Phi_0 - \Phi$) divided by the incident radiant power Φ_0, or

$$\alpha = \frac{\Phi_0 - \Phi}{\Phi_0} \tag{3-16}$$

The absorption factor α is related to the atomic absorption coefficient K, in cm^{-1} or m^{-1}, by Beer's law:

$$\alpha = 1 - \exp(-KI) \tag{3-17}$$

where l is the absorption pathlength (cm or m). The atomic absorption coefficient K can be written in terms of population density n_i (atoms cm^{-3}) of the lower level,

absorption oscillator strength f_{ij} and spectral profile function S by

$$K = \frac{e^2 S n_i f_{ij}}{4 \varepsilon_0 m_e c} \qquad (3\text{-}18)$$

where e is the charge of electron, ε_0 is the permittivity of free space, m_e is the mass of the electron and c is the speed of light. Finally, the absorbance A can be rewritten as

$$A = -\log T = -\log(1-\alpha) = 0.434\ K\ l \qquad (3\text{-}19)$$

In this work, a spreadsheet from the MATHCAD software (version 4.0, MathSoft Inc., Cambridge, Massachusetts) was used to calculate the absorption profile of Rb metal vapor filter at different temperatures. The detailed procedures to simulate the approximation of Puerta and Martin's Voigt spectral profile function are summarized below.

Because of its role in absorbing the laser specular scatter, the Rb metal vapor filter is one of the most critical component to detect a single molecule flowing in a capillary. Rb atom has two main isotopes, ^{85}Rb and ^{87}Rb, which exist naturally in the ratio of 0.727 0.273 [9]. The fact that rubidium element contains more than one isotope in natural abundance causes lines in the spectra to appear as multiples (hyperfine structure). The melting point for Rb is 39 °C, so it is easy to produce a sufficient number density of atoms at a moderate temperature range. The energy levels involved in the hyperfine transitions of Rb at 780.023 nm are

shown in Figure 3-3.[96] In this figure, F is the quantum number associated with the total angular momentum , which includes those due to orbital and spin motion of the electrons and spin motion of the nucleus. The components of the hyperfine transition are numbered for easy reference. The resonance lines consist of 4 groups of components, 2 groups for each isotope. The relative intensity and relative position (in pm and cm^{-1}) for all hyperfine transitions are given in Table 3-3.[96]

Various approaches have been used to estimate the vapor pressure (number density) of Rb atoms at different temperatures.[97] From measurements of optical absorption of the resonance lines, Gallagher et al. had been able to precisely determine the vapor pressure (number density) of Rb at different temperatures.[96] The vapor pressure or number density can be described as

$$\log(p) = -\frac{A}{T} - B\log(T) + C + DT \qquad (3\text{-}20)$$

$$\log(N) = \frac{A}{T} - (B+1)\log(T) + C + DT + 18.985 \qquad (3\text{-}21)$$

where p is vapor pressure in Torr, N is number density in cm^{-3}, A=4529.6, B=2.911, C=15.8825, and D=0.0059. Figure 3-4 shows the calculated number density of Rb atoms from 20 °C to 200 °C. At 100 °C, the number density of Rb atoms is calculated to be 5.12×10^{13} cm^{-3} which is close to the experimental value.[97] The collisional cross section σ_c for N_2 is 2.49×10^{-19} m^2.[96] The number density of the

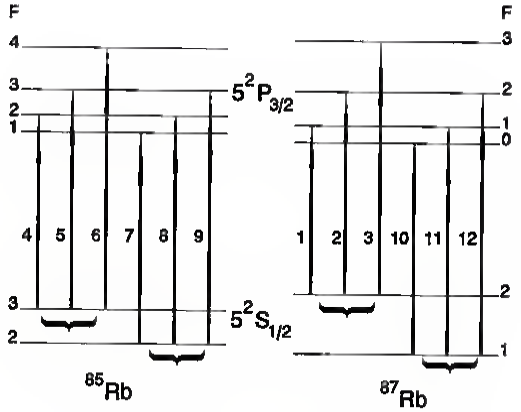

Figure 3-3 Energy-level diagram of Rb 780 023 nm (not to scale).

Table 3-3 Intensities and positions of the rubidium hyperfine structure

Component	Relative Intensity	Relative Position (pm)	Relative Position ($x10^{-3}$ cm^{-1})
1	0.026	+0.085	-14.05
2	0.133	+0.540	-6.66
3	0.374	+0	0
4	0.123	-1.901	31.25
5	0.432	-2.043	33.58
6	1	-2.286	37.58
7	0.333	-7.979	131.15
8	0.432	-8.064	132.55
9	0.346	-8.198	134.75
10	0.053	-12.870	211.55
11	0.133	-13.014	213.90
12	0.133	-13.334	219.17

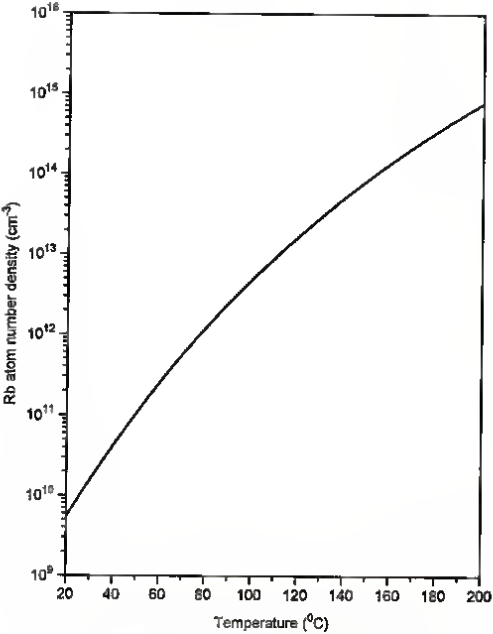

Figure 3-4 Calculated Rb number density at different temperatures

collisional partners, N_2, also can be estimated from the pressure within the Rb MVF at different temperatures. The collisional broadened linewidth, $\Delta\nu_L$, and Doppler broadened linewidth, $\Delta\nu_D$, for each hyper-fine transition line are obtained from equation (3-4) and equation (3-7), respectively. It is quite straightforward to compute the shape of all Rb transitions consisting not only of a single line, but also, as in our case, of 3 lines per group. For each frequency point, the absorption coefficient K is calculated for every line and integrated over all lines with the Voigt spectral profile function S which is approximated by J(d, p) (see equation (3-12)) in our case. Figure 3-5 shows the theoretical absorption coefficient **K** of the Rb 780 023 line including hyperfine structures and the relative intensity of the two Rb isotopes. Afterwards one can compute the absorbance **A** for an absorption pathlength l by the simple relation given in equation (3-19). Figure 3-6 shows the calculated Voigt absorption profile, a convolution of Gaussian and Lorentzian profile functions, of Rb at 27 °C, 50 °C, and 100 °C. As Figure 3-6 shows, increasing cell temperature has a large effect on the absorbance, which essentially mirrors the increasing Rb metal vapor number density. The presence of more than one peak for each absorption profile is due to the hyperfine structures of the overall transition. The Voigt absorption bandwidth is estimated to be 21 pm at 780 023 nm which is close to the measured absorption bandwidth [7]. Ideally, once the narrow laser line is tuned to the absorption peak of the Rb MVF at 100 °C, an absorbance of several thousand could be reached.

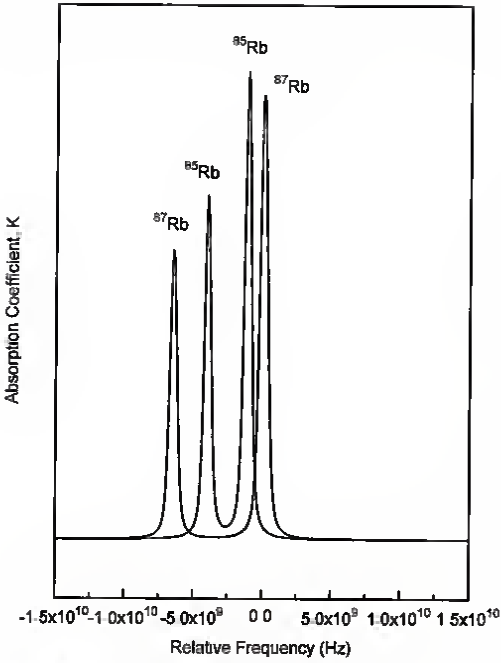

Figure 3-5 Absorption coefficient K for ^{85}Rb and ^{87}Rb

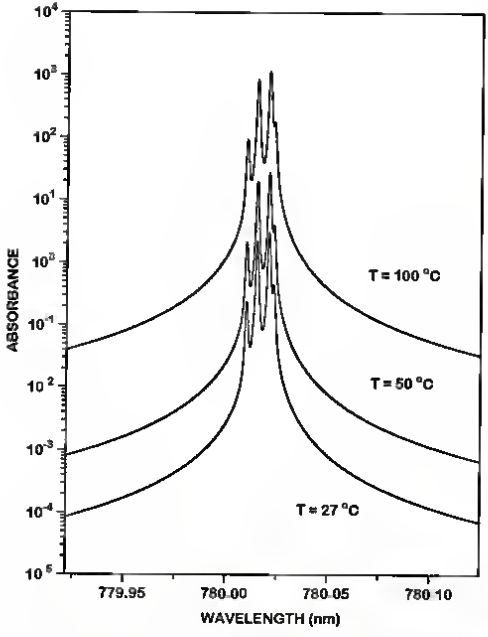

Figure 3-6 Calculated absorption profile of Rb MVF at different temperatures

CHAPTER 4
EXPERIMENTAL

General Experimental Configuration

The general LIF-MVF system for single molecule detection is shown in Figure 4-1. Table 4-1 gives a detailed listing of experimental components. All-line outputs from an argon ion laser are used to pump a single-mode, tunable, continuous wave Ti:sapphire laser in the ring configuration. The sample is confined in a capillary and flow is controlled by a mechanical microliter syringe pump. The laser is focused onto the uncoated part of the capillary with a beam expander and a camera lens. The fluorescence and laser scatter from the capillary are collected at right angles by a microscope objective (MO1), and passed through a rubidium metal vapor filter to absorb the laser scatter. The fluorescence is then refocused by the other microscope objective (MO2) onto an optical fiber pigtail which is prealigned to a single photon avalanche photodiode. The digital output pulses from the single photon avalanche photodiode are then interfaced to a computer-controlled counter/timer board. Detailed information including design and performance of each component is discussed in the following sections.

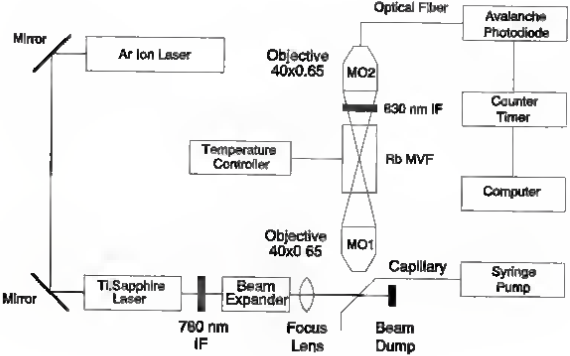

Figure 4-1 Near-IR single molecule detection apparatus

Table 4-1 List of experimental components.

Component	Manufacturer
Argon Ion laser	Spectra Physics 2060, Mountain View, CA
Ti sapphire laser	Schwartz Electro-Optics, Inc., Orlando, FL
Excitation filter	Omega Optical, Brattleboro, VT
Fused Silica Capillary	Polymicro Technology, Phoenix, AZ
Mechanical Microliter Syringe Pump	Harvard Apparatus 975, South Natick, MA
Beam Expander	Melles Griot, Irvine, CA
Microtranslational Stage	Newport 461-XY-M, Irvine, CA
Rb Metal Vapor Filter	Opthos, Rockville, MD
Furnace	Lindberg 55035, Watertown, WI
Band Pass Interference Filter	Corion Hollston, MA
Microscope Objective	Melles Griot, Irvine, CA
Single Photon Avalanche Photodiode	EG&G Optoelectronics Canada SPCM-200, Veudreuil Canada
Counter/Timer Board	Keithley Metrabyte CTM-05, Taunton, MA
IR140	Exciton Chemical Co., Inc , Dayton, OH
Methanol	Optima Grade, Fisher Scientific, Orlando, FL

Argon Ion Laser Pumped Tisapphire Laser System

In this work, the requirements for the LIF MVF system capable of single molecule detection are

(1)the laser irradiance (W/cm^2) must be sufficient to obtain a reliable signal from single molecules while passing through the laser beam

(2)the laser wavelength must be tuned to the absorption peak of MVF and must excite the fluorophor efficiently.

(3)the laser line should have a Gaussian profile with a linewidth less than the absorption bandwidth of MVF.

(4)the laser must be cw or pulsed with a repetition rate sufficiently high that each molecule interacts with at least one laser pulse while passing through the observation region

Among all light sources currently available, the Ti sapphire laser has the best characteristics for single molecule detection.

The Ti sapphire ($Ti:Al_2O_3$) laser was first demonstrated in 1982, and the commercial cw models were available in 1988 [71,72]. A Ti sapphire laser offers many of the same features as near-IR dye lasers. The absence of a flowing dye solution greatly enhances stability, reduces noise by a factor of 10, and allows a linewidth as narrow as 1 kHz in a ring configuration.

The Ti sapphire laser uses crystals of sapphire doped with roughly 0.1% Ti, added as the Ti^{3+} ion, which replaces aluminum (Al^{3+}) in the crystal lattice [73,74,75,76]. The Ti^{3+} ion is in the same class of 3d transition metal ions that include Cr^{3+} and

Co^{2+}, which are used in other vibronic solid-state lasers. Like ruby, which is Cr^{3+} Al_2O_3, Ti sapphire crystals are hard and durable with good optical properties The laser transition is between the ^2E excited state and the $^2T_2$ ground state. Optical pumping excites Ti^{3+} to the upper laser level, which then relaxes to the bottom of the vibronic band before making the laser transition (see Figure 4-2) Vibrational relaxation then drops the ion to the bottom of the ground vibronic band A strong interaction between the titanium atom and host crystal, combined with the large difference in electron distribution between the two energy levels, makes the transition linewidth broad

Absorption and emission bands of Ti:sapphire overlap only slightly Absorption peaks near 500 nm - a wavelength readily available from argon ion laser, frequency-doubled neodymium laser, or copper-vapor laser All three lasers have been used as pump sources for Ti sapphire laser The fluorescence peaks at 780 nm, but Ti sapphire output is readily tunable, with a maximum power at 700 - 900 nm.

The typical design of the Ti sapphire laser in the ring configuration is shown in Figure 4-3. Table 4-2 lists the specifications of the commercial Ti sapphire laser purchased for use in this project.[77] When pumped by the all-lines output of an argon-ion laser, Ti sapphire lasers provide watt-level CW, tunable radiation over the wavelength region from 680 nm - 1130 nm The Gaussian spectral linewidth is less than 40 MHz in the ring cavity which corresponds to less than 0 084 pm at 780 023 nm Rb transition Since the absorption bandwidth of Rb MVF at 100 °C

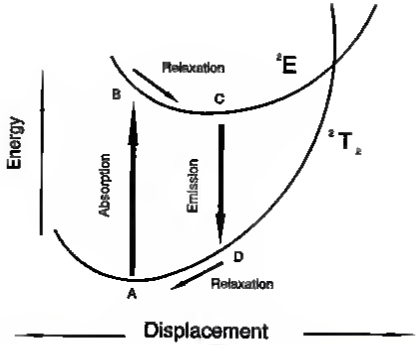

Figure 4-2 Ti sapphire laser is optically excited (B), then relaxes to the upper laser level (C). Laser emission leaves the ion in a vibrationally excited sublevel of the ground state (D), which relaxes back to the ground state

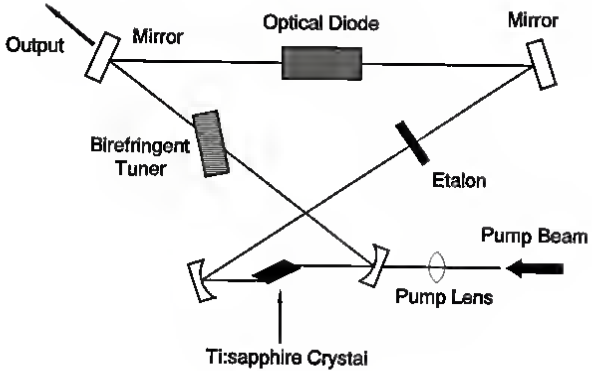

Figure 4-3 Ti:sapphire laser in ring configuration

Table 4-2 Specifications of Ti sapphire laser.

Parameter	Specific Value
Maximum power (at 800 nm)	750 mW
Tuning range	680 nm - 1130 nm
Spectral linewidth	< 40 MHz at ring configuration
Spectral profile	Gaussian
Spatial profile	TEM_{00}
Polarization	Horizontal
Beam size	1 mm at exit

is approximataly 21 pm [78] the laser line should be totally absorbed by the Rb MVF once the laser is tuned to Rb absorption peak

The Ti sapphire laser is a passive device requiring a pump laser to initiate the lasing action The argon-ion laser contains a beam lock positioning system to provide excellent beam pointing characteristics which determine the output-power stability of Ti:sapphire laser [78] The beam from the argon ion laser is locked onto a reference point beyond the resonant cavity When the beam moves, the output mirror responds to restore position. The Ti:sapphire laser is a tunable solid state laser containing the Ti:sapphire crystal and several optimized mirror sets (see Figure 4-3). Depending on the pump laser power, the conversion efficiency of Ti:sapphire laser is at least 10% A weak, broad-band Ti:sapphire crystal fluorescence, collinear with the laser beam, is further attenuated with a excitation interference filter Figure 4-4 shows the measured spectral profile (by manufacturer) of this excitation interference filter with FWHM=0 18 nm centered at 780 0 nm.[79] To maximize the transmittance, this interference filter is tilted at some angle after the Ti sapphire laser is tuned to the Rb line at 780.1 nm.

Near Infrared Dyes

In recent years, the use of near-IR dyes as fluorescent probes has been of great interest in biomedical applications [80] Traditionally, visible fluorescent probes provide a sensitive method to obtain information about the structure, function, and health of cells.[81] These visible dyes are generally stable compounds with

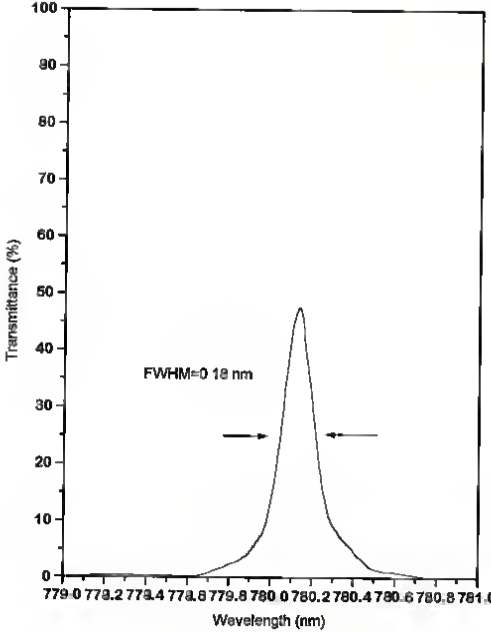

Figure 4-4 Spectral profile of excitation filter

absorption maxima conducive to argon ion laser excitation (514 nm and 488 nm). However, their spectral properties are in a region that is susceptible to bio-interference which can greatly increase the detected background. For example, Raman scatter and background fluorescence due to optical materials and solvent cause considerable difficulties in minimizing the background noise.

All dyes which emit between 690 nm and 1100 nm will be called near-IR dyes. The use of near-IR fluorescent probes is attractive. First, absorption of solvents and optical materials in the near-IR region is small or negligible. Second, the fluorescent background due to concomitants is small or negligible and photodestruction (photobleaching) is generally less severe than the visible dyes. Third, many near-IR dyes have significant molar extinction coefficients (ε) and high fluorescent quantum efficiency (Q_f). Fourth, only a small group of polymethine dyes are fluorescent above 750 nm, and very few such compounds exist in the environment thus minimizing interferences at the excitation wavelength. Patonay's group have been leaders in the development and use of near-IR fluorogenic labels for biological important molecules.[52,53,54,55,56] Imasaka et al.[25] as well as Akiyama[57] and Lahotay, et al.[24] have also used diode laser excitation of near-IR fluorophores.

The ideal near-IR dyes for single molecule detection will have the following characteristics.

(1)strongly absorb at the laser excitation wavelength ($\varepsilon \geq 10^5$ L M^{-1} cm^{-1}).

(2)strongly fluoresce ($Q_f \geq 0.25$).

(3)excite and fluoresce at wavelengths where background fluorescence

is negligible

(4)excite and fluoresce at wavelengths that Raman scatter of the solvent is not within the fluorescence band.

(5)excite at a wavelength which can be effectively absorbed by a MVF

Very few chemicals fluoresce in the near-IR region. Patonay and Antoine have reviewed the major near-IR fluorophor labels.[88] The Patonay group has also synthesized many new and improved near IR dyes.[89] Such near-IR dyes can be either covalently or non-covalently attached to molecules of interest.[90] Covalent attachment is possible through functional groups, such as NCS, that bond directly to NH_2. Non-covalent attachment is nonspecific binding through adsorption or electrostatic forces. The only near-IR dyes that satisfy the above criteria are the cyanine dyes, known as polymethines. These polymethine dyes that absorb at wavelengths $\geq$ 670 nm have high quantum efficiency and good solubility in aqueous and/or near aqueous solutions. Table 4-3 is a list of polymethine dyes which are soluble in water, DMSO and/or methanol.[91] These near IR dyes have highly conjugated, semi-symmetrical structures containing several aromatic rings with the length of the structure correlating to their fluorescent characteristics.[91]

Three polymethine dyes, IR125, IR132, and IR140, are potentially useful for single molecule detection with excitation at 780.023 nm. Figure 4-5 gives the structures of these three polymethine dyes. Ultrasensitive near-IR detection of IR140 in methanol has been reported using a diode laser as the excitation source.[23,24] The lifetime of IR140 ($\epsilon = 1.5 \times 10^5$ L/mol cm) is measured to be 791±17

Table 4-3 Near IR fluorescence dyes possible use in the single molecule detection

Dye	Molecular Formula	λ_{ex}(nm)	λ_{em}(nm)
Nial Blue A perchloate	$C_{30}H_{29}N_3OClO_4$	627	660
Methylene Blue	$C_{16}H_{18}N_3SCl$	668	683
DTDC	$C_{29}H_{23}N_2S_2$	652	679
Oxazine 750	$C_{34}H_{31}N_2OCl$	673	691
Rhodamine 800	$C_{28}H_{28}N_2OCl$	682	700
DOTC	$C_{29}H_{28}N_2O_2$	695	719
Cryptocyanine	$C_{32}H_{48}N_2O_4S_2ClO_4$	717	729
IR144	$C_{50}H_{56}N_4O_2S_2NEt_3$	744	825
HITC	$C_{29}H_{33}N_2I$	750	790
DQDC	$C_{27}H_{27}N_2$	765	835
DDTC	$C_{32}H_{29}N_2$	765	855
DTTC	$C_{23}H_{25}N_2S_2$	772	820
HDITC	$C_{36}H_{37}N_2ClO_4$	780	828
IR125	$C_{34}H_{47}N_2S_2Na$	795	833
DQTC	$C_{39}H_{33}N_2$	825	865
IR140	$C_{28}H_{34}Cl_2N_2S_2ClO_4$	826	882
IR132	$C_{28}H_{46}N_2O_4S_2ClO_4$	832	905

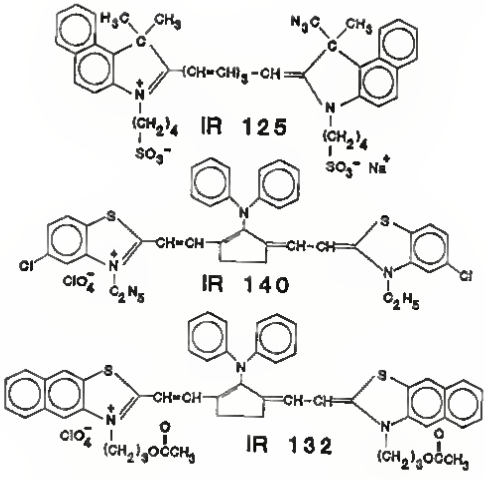

Figure 4-5 Chemical structure of the polymethine dyes IR125, IR140, and IR132.

ps with a fluorescence quantum yield (Q_f) close to unity.[62] Due to these optical characteristics, IR140 with excitation at 780.023 nm (Rb transition line) is emphasized for single molecule detection.

Sample solutions at different concentrations are prepared by serial dilution of a 1.5×10^{-3} M stock solution and analyzed on the same day. All glassware used to contain the sample solution are kept in a NOCHROMIX (Godex Laboratories, Inc.) cleaning solution (mixed with sulfuric acid) and then rinsed thoroughly with water and methanol.

Capillary Flow Cell

An ideal system for sample containment should not perturb the analysis and introduce noise during the measurement. A sheathed flow cuvette and electrodynamically levitated microdroplets have been applied to contain the analytes for single molecule detection (as discussed in Chapter 1). However, both techniques require sophisticated experimental optimization to confine the sample in a flowing stream or to suspend the molecules in a microdroplet.

The capillary flow cell is simply a glass or quartz tube requiring no instrumental adjustment. Capillaries of various sizes are commonly used in several types of chemical separation techniques, including packed capillary liquid chromatography, open tubular capillary liquid chromatography, and capillary electrophoresis. The sample is introduced at one end of the capillary and thereafter forced through the capillary by means of pressure or electric field. UF

detection is performed on a bare portion of the capillary column. A major advantage of on-column capillary detection is that it facilitates the analysis of an extremely small probe volume, nL to pL range, which is desirable in the reduction of Raman scatter from the solvent. The extremely small physical dimensions encountered in the capillary column also require that the detection be performed on column, which excludes the utilization of external flow cells, such as a sheathed flow cuvette.

In this work, the capillary was filled with laser radiation to assure 100% spatial probing efficiency which is difficult with uv-visible excitation because of laser scatter and background noise. The ability to focus the laser beam with preserved intensity to a diffraction-limited spot size has permitted nanoliter to picoliter probe volumes within the flow cells. Furthermore, the high spatial coherence of many CW lasers makes it possible to produce a beam-center irradiance in a tight focus that may even be sufficient to permit optical saturation of the fluorescence. The metal vapor filter has an excellent capability for laser scatter rejection and, therefore, allows filling of the capillary column with laser light to achieve 100% measurement efficiency.

The design of the flow cell prepared from the fused silica capillary tubing is shown in Figure 4-6. In order to prevent the room light from reaching the detector, the capillary flow cell was held rigid inside a small metal dark box (5 cm x 5 cm x 5 cm). To have a small probe volume, the capillary with smallest inside diameter (ID) should be the best choice for single molecule detection.

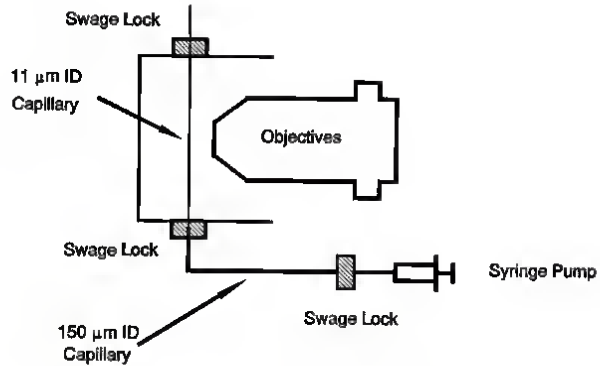

Figure 4-6 Cut-away view for the design of capillary holder.

Unfortunately, those capillaries with ID (inner diameter) less than 5 μm can not be used due to the uncertainty in capillary inside diameter (deviation > 50%). Also, because of the back pressure from the capillary and the geometric limitations of the dark box, a capillary with a 5 cm length and a 11 μm inside diameter (deviation < 10 %) is selected as the sample containment vessel.

To create a fluorescent window in which the sample can be excited, a small part of the polyimide coating on the fused silica capillary tubing must be removed. There are various techniques available to remove the polyimide. The thermal methods apply arc or filament sources to burn off the polyimide coating but leave a sooty layer on the capillary. The open flames from torch, lighter, and matches work but do leave the glass brittle. Strong bases will remove the polyimide, but they also affect the silica material, resulting in brittle glass. When compared with other techniques, concentrated sulfuric acid at 100 °C will remove the polyimide in a few seconds and leave no brittle glass. Therefore, the hot acid method is used to create the fluorescent window on the capillary for single molecule detection.

The sample solution is pumped through the capillary flow cell with a mechanical microliter syringe pump. The quality of this pump starts with a quiet precision instrument motor, which is synchronous - that is, its speed is regulated by the supply line frequency, which is normally within ±0.01% accuracy. By infusing a small volume of solution with a gas tight microliter syringe, the measured flow rate is very similar to the value specified from the manufacture. For example, by using a 100 μL syringe, the flow rate is able to be varied by at least four order-

of-magnitude from 1.25 μL/min to 0.000102 μL/min with very high precision and accuracy. To obtain a stable slow flow rate, 30 - 60 minutes waiting time is normal for the motors to "catch-up" before making the measurement.

To avoid a clogging problem, it is critical to have clean connections for the capillaries with small inside diameter. In chromatography, different types of ferrules have been developed for making glass to-metal and glass-to-glass connections. Unlike soft graphite, vespel ferrules are chemically inert and suitable for glass to metal connections. They do not soften or melt, nor lose their physical integrity at high temperatures. Vespel ferrules will not produce particles when compressed. Therefore, vespel ferrules are used for capillary connections through the sample injection system.

Laser Focusing

Since the inside diameter of the capillary is very small, it is important to have a fine alignment of the focusing optics on capillary. The detailed procedures to focus the laser beam on the capillary are described below.

First, remove both the beam expander and focus lens and position the capillary at the center of the unfocused laser beam. Because the laser is hindered by a capillary, a straight line should be seen within the round laser spot as shown in Figure 4-7. Second, replace and translate the focus lens across the capillary until a symmetric strip-shape diffraction pattern appears (as seen in Figure 4-8). Third, replace and position the beam expander and make sure the expanded laser

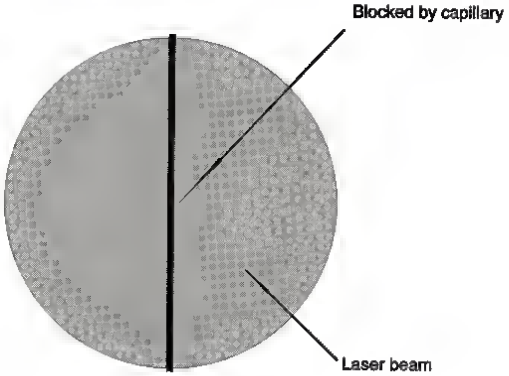

Figure 4-7 Image of procedure 1 in laser focusing.

Figure 4-8 Image of procedure 2 in laser focusing.

beam passing through the center for focus lens. Fourth, adjust the focus lens to the near focus position. If in the right focus, a symmetric round-shape diffraction pattern with a bright spot in center should be seen (as seen in Figure 4-9).

Light Collection

There is a simple way to align the light from the capillary to the detector. A He-Ne laser beam is sent to one end of an optical fiber and passed through the focusing microscope objective (MO2). By positioning the collecting microscope objective (MO1), intense laser scatter can be seen from the capillary. This finishes the rough alignment of the collecting optics. The MO2 and optical fiber are then removed. After the Ti:sapphire laser is tuned off 780.023 nm, the laser beam is sent to the capillary. By positioning the MO1, a clean, sharp image of scatter caused by the capillary wall (Figure 4-10) can be seen with an IR viewer after the metal vapor filter.

Rubidium Metal Vapor Filter

The commercially available metal vapor cell (see Table 4-1) consisted of a quartz cylindrical cell (length = 10 cm and diameter = 2.5 cm) with parallel quartz windows on both ends. An excess of rubidium metal (500 mg) is distilled into the evacuated cell such that sufficient amount of metal would be present to give saturated metal vapor at all temperature range used in this work (room temperature to 170 °C). Nitrogen gas at 200 Torr (at room temperature) is used

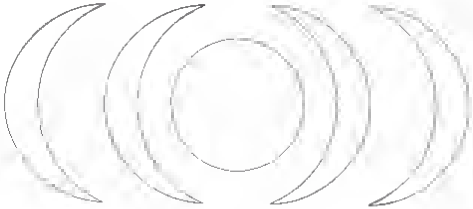

Figure 4-9 Image of procedure 3 and 4 in laser focusing.

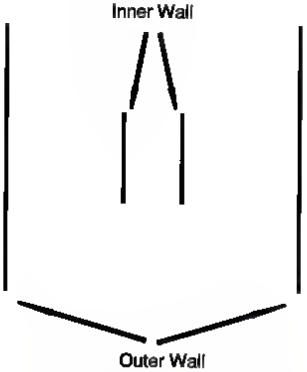

Figure 4-10 Image of scattered light from the capillary wall.

as the fill gas in order to quench the atomic resonance fluorescence and broaden the absorption bandwidth of the Rb MVF. To avoid the window discoloring problem due to attack of hot Rb metal vapor, the Rb MVF is held inside a cylindrical forced hot nitrogen heating device, as shown in Figure 4-11. The outside of the heating device is wrapped with a heating tape to improve the heating efficiency. The heated nitrogen from the furnace, whose temperature was controlled to within ±1 °C, flows past both windows and recycles back to the body of the MVF. In this way, the flat window faces of the MVF will be kept warmer than the center of the MVF. This prevent the metal vapor from condensing onto the windows, which will reduce the signal throughput and the transmittance of the MVF. Therefore the problem due to rapid window damage can be avoided. Actually, the Rb metal vapor filter used in this work has functioned flawlessly for over one year.

Spectral Filter

Laser specular scatter occurs in all directions arising from both the outer and inner walls of capillary. Despite the ability of the MVF to absorb the laser specular scatter, other noise sources may generate a formidable problem for single molecule detection. Therefore, additional spectral filters are required to further reduce the background noises.

Rayleigh scatter from the molecules in the quartz capillary is very weak and occurs at the same wavelength as the laser emission. However, this form of

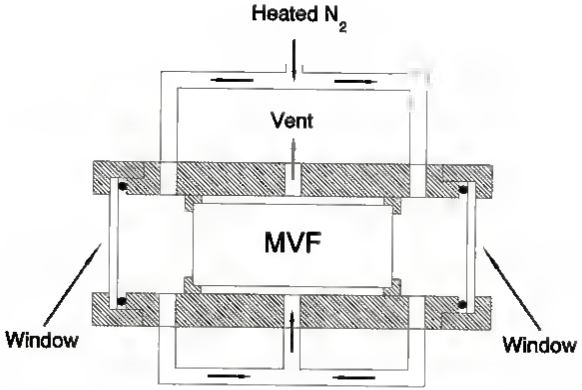

Figure 4-11 Cut away view for the design of metal vapor filter

scatter is expected to be negligible due to the small capillary volume illuminated and the broadened absorption profile of Rb metal vapor filter

For the LIF on-column capillary detection, the quartz capillary and solvent are the two main sources of Raman scatter. Quartz has a Raman emission band at 464 cm^{-1} which corresponds to 809 nm for 780.023 nm excitation. Lehotay has discussed the effect of different solvents on background signal and found that methanol has a Raman peak at 865 nm when excited at 780.023 nm.[35] Three polymethine dyes (IR125, IR132, and IR140) to be tested in this project have broad fluorescence bands from 800 nm to 850 nm when excited at 790.023 nm. To block the Raman scatter sources, several band pass interference filters (see Table 4-5) are placed before the detector to optimize the S/N ratio for single molecule detection.

Detector and Data Acquisition

Ultrasensitive detection and photon counting experiments require a detector with high quantum efficiency, low dark noise, fast response time, and good single photon detection capability. In previous experiments for the detection of single molecules in solution, photomultipliers (PMT) have been used to achieve most of these requirements except that the quantum efficiency was only 5%-8%. However, due to recent improvements in solid state semiconductor photodetector, considerably higher quantum efficiency, together with adequate time response and low dark count rate, can now be provided by a single photon avalanche

Table 4-5 The interference filters to be used in single molecule detection

Filter	Center Wavelength (nm)	Band Width (FWHM, nm)	Minimum Peak Transmittance
S-10-800	800 ± 2	12 ± 2	45%
S-10-810	810 ± 2	12 ± 2	45%
S-10-820	820 ± 2	12 ± 2	45%
S-10-830	830 ± 2	12 ± 2	45%
S-10-840	840 ± 2	13 ± 2	45%
S-10-850	850 ± 2	13 ± 2	45%

photodiode.

Because of its simplicity, smaller size, and ease of operation, the single photon avalanche photodiode (SPAPD) has the potential for becoming the device for applications in lidar, photon correlation spectroscopy, optical fiber test, fluorescence lifetime measurements, and ultrasensitive spectroscopy, where the light being measured can be focused to a small spot.

The SPAPD is a self-contained module which detects single photons of light over the wavelength range from 400 nm to 1060 nm, a range and sensitivity which often outperforms PMT. The specifications of an SPAPD are given in Table 4-6 [8]. Exhibiting a linear response range over more than 6 decades, the SPAPD is an integrated detector module capable of single photon detection with sensitivity comparable to that of a PMT. The SPAPD is a solid-state device which requires only a short settling time after photon-saturation, in contrast to PMTs, in which several hours of recovery time are often necessary after exposure to intense illumination. At higher incoming light levels the count rate actually decreases. As an extreme example, if the SPAPD is exposed to room light, the count rate will fall to zero. Figure 4-12 shows the measured recovery time of an SPAPD after exposure to room light. It is found that the SPAPD needs about 2 minutes to reach a stable signal. The detector module has an unique silicon avalanche photodiode which has a circular active area whose peak photon detection efficiency, within 50 μm of the center, exceeds 40% at 633 nm. The photon detection efficiency at 830 nm specified from the manufacture is 25%. Since the

Table 4-6 Specifications of single photon avalanche photodiode

Electrical Characteristics	Minimum	Typical	Maximum
Supply Voltage Required +12 @ 0 08 A max +5 @ 1 3 A max -5 @ 0 02 A max	 11 9 V 4 9 V -4 9 V	 12 0 V 5 0 V -5 0 V	 12 1 V 5 1 V -5 1 V
Supply Voltage Ripple (rms)	-	-	50 mV
Case Operating Temperature	5 °C	-	40 °C
Photon Detection Efficiency (P_d) λ = 1060 nm λ = 830 nm λ = 633 nm λ = 400 nm	 - 25 % 40 % -	 1 3 % 32 % 46 % 15 %	 - - - -
Photon Detection Efficiency Variation at Constant Case Temperature	-	± 1 %	± 3 %
Photon Detection Efficiency Variation from 5 °C to 40 °C compared with 25 °C Case Temperature	-	± 5 %	±10 %
Dark Count (counts/s)	1 - 3	≤ 25	100
Dark Count Variation at Constant Case Temperature	-	± 2 %	± 10 %
Dark Count Variation from 5 °C to 40 °C compared with 25 °C Case Temperature	-	± 5 %	± 15 %
Dead Time	-	200 ns	-
Output Count Rate Before Saturation (counts/s)	$1.3x10^5$	$1.8x10^7$	-
Single Photon Timing Resolution	-	3 ns	-
Settling Time Following Power up	-	20 s	100 s
Threshold Setting Required for Digital Output Pulse	0.5 V	1.0 V	1.5 V

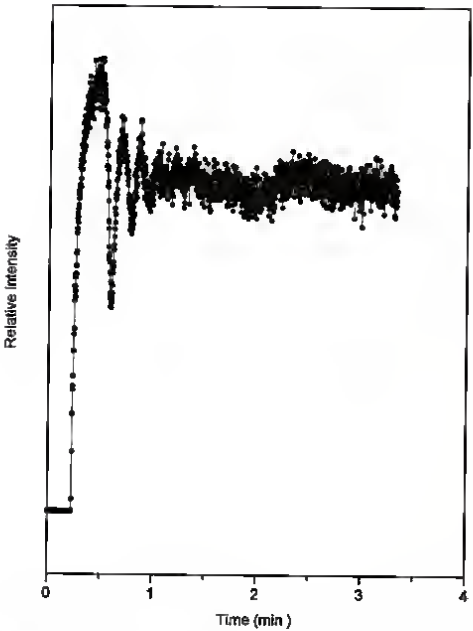

Figure 4-12 The recovery time of en SPAPD after exposure to room light.

dark noise of the device is proportional to its active area, the detector size is minimized. Typical dark count rate is approximately 25 counts/s. Temperature regulation is provided by an integrated thermoelectric device. The detector module contains a passive quench circuit capable of photon counting up to 1.8×10^7 counts/s, with single photon timing resolution of 3 ns rms. There is a "dead time" of 50 ns between photon pulses. The SPAPD is temperature controlled, ensuring stabilized performance despite changes in the ambient temperature. In addition, the high-voltage supply is integrated into the detector module, thus avoiding the risk of exposure to the dangerous electric fields encountered with PMT. The detector module requires only low-voltage inputs, +12 V (0.08 A max), +5 V (1.3 A max), and -5 V (0.2 A max). The low power requirement of the SPAPD and the solid-state nature of the device suggest the possibility of battery-power operation and the ready transportation of the instrument from the laboratory into a more stringent environment. A digital TTL pulse, 2 V high and approximately 200 ns wide, is the output at the BNC connector as each photon is detected.

To measure the photon burst from single molecules, the instrument employs an IBM AT-compatible counter/timer board to count the digital TTL pulse train provided by the detector module (SPAPD). The counter/timer board is housed in a 386 computer with 80387 math co-processor. The computer is also used for counting control, spectral data processing, and display. A computer program, used to control the counter/timer board, was written in the QUICK BASIC language. To test the performance of the detector, count rate is measured at

different laser powers (see Figure 4-13). The SPAPD is able to count the photon flux precisely up to $1x10^6$ counts/s. At high input photon fluxes, the SPAPD become saturated due to dead time and electronic limitations.

In order to collect a number of data points per molecular transit time, the counting interval (time segment) must be less than the transit time of a single molecule. The accuracy of the counter/timer board can be tested by calibrating with a standard TTL pulse generator. The ratio of measured count rate to input count rate at different integration times is shown in Figure 4-14. The counter/timer board is able to count signals with sampling intervals from 200 μs up to at least 2 ms with near unity accuracy. The performance becomes degraded when the sampling time interval is less than 200 μs. The 200-μs integration time should be enough to measure the photon burst from single molecules with a 1 ms transit time in this project (5 data points per transit time).

Tuning the Laser to Rubidium Absorption Line

In order to tune the Ti sapphire laser to the Rb transition line at 780.023 nm, the Rb MVF is heated to 100 °C and the laser scatter from the capillary is passed through the Rb MVF onto the detector. The Ti:sapphire laser is tuned to maximum absorbance of Rb MVF by slowly adjusting the intracavity birefringent filter. Fine tuning is done by tilting the intercavity Fabry Perot etalon to further maximize the absorbance. The maximum absorbance is more like a plateau than a peak because the Fabry Perot etalon can be adjusted significantly before the laser is

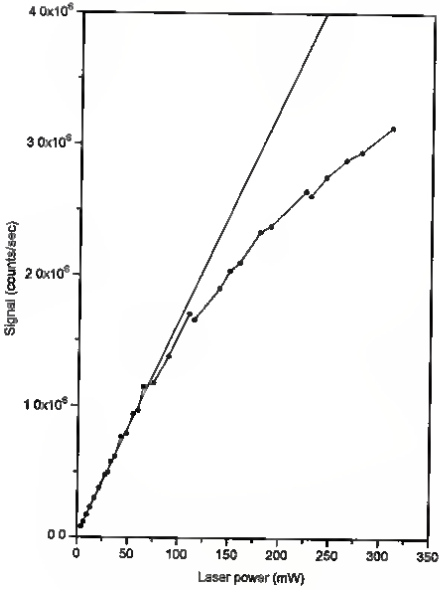

Figure 4-13 The measured counting rate of SPAPD

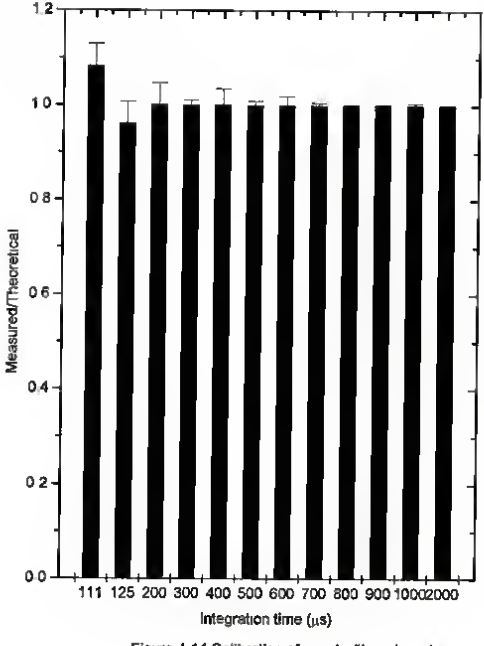

Figure 4-14 Calibration of counter/timer board

tuned off-wavelength and the absorbance decreased sharply. The calculated laser linewidth (FWHM) at 780.023 nm is less than 0.081 pm when the Ti:sapphire laser is operated in ring configuration with 40 MHz spectral line width. Occasionally, the laser frequency would jump away from the Rb transition line. This rarely occurred if the birefringent filter were set to the center frequency of the etalon after the laser has been operating for more than 30 minutes. Once this operation has been is carried out, the laser has excellent day-by-day frequency stability.

CHAPTER 5
RESULTS AND DISCUSSION

Optical Optimization

To minimize the laser specular scatter reflected from the capillary wall, the positions of laser focusing and signal collecting optics were optimized to find the best signal-to-noise ratio. For easy reference, laser was propagated on the X-axis, fluorescence was collected on the Y-axis, and the flow of molecules was in the Z-axis. The effects of the position of the focusing lens on the fluorescence signal and laser scatter are shown in Figure 5-1. The maximized fluorescence signal was obtained when the capillary was within the focus region of laser beam. By positioning the focus lens across the capillary, Figure 5-2 shows how the fluorescence intensity and elastically scattered light varied with the lateral position of the laser beam for a 11-μm capillary flow cell. The laser scatter increased rapidly when the beam was moved away from the center of the capillary. This implies that the best S/N ratio is obtained when the beam is incident on the capillary center.

By translating the collecting microscopic objective (MO1) near the capillary, Figure 5-3 shows the measured fluorescence signals obtained at different positions. This plot gives the field of depth of a microscopic objective. Since the

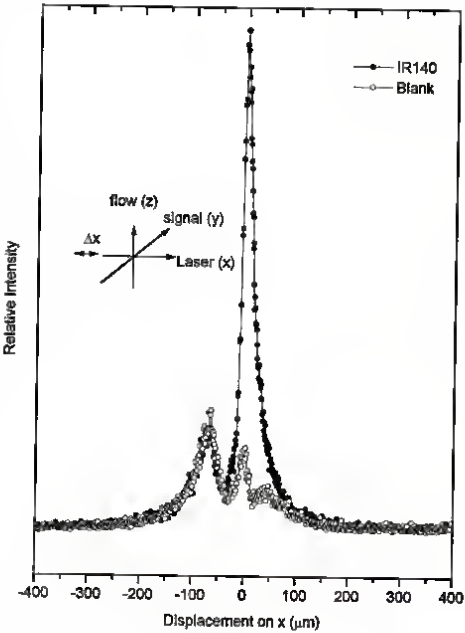

Figure 5-1 Effect of focusing lens on fluorescence and scattered light

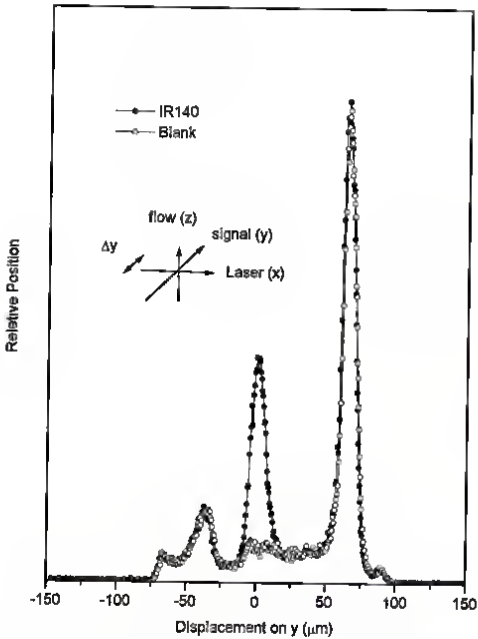

Figure 5-2 Effect of focusing lens on fluorescence and scattered light

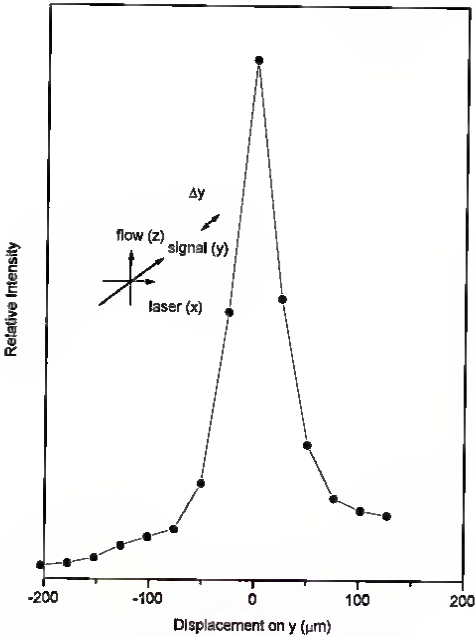

Figure 5-3 Effect of collecting microscope objective (MO1) on fluorescence

capillary has 140-μm OD and 11-μm ID the estimated distance for maximum fluorescence signal is approximately 400 μm from the center of capillary To optimize the lateral position, the MO1 was translated horizontally across the capillary at the distance of best field of depth Figure 5-4 shows how the fluorescence signal varied with lateral position of MO1 for e 11- μm ID capillary flow cell This is known as the field of view of the microscopic objective

To evoid the diffraction effect between the capillary and the laser beam, the fluorescence profiles from the capillary were evaluated at different focus positions. By translating the MO1 laterally at the best field of depth, the fluorescence profiles recorded at various positions of the focus lens are shown in Figure 5-5. In from of the focal plane of the focus lens (near-field), the profiles are skewed into two side-lobes These depict the near-field diffraction effects due to constructive and destructive interference between the waves geometrically transmitted from the capillary (like an aperture) and the spherical waves produced at the edges of capillary inside diameter Beyond the focal plane of the focus lens (far-field), the profiles have a symmetrical shape The changes of fluorescence profiles from the near-field to far field suggest that signal collection should be performed in the far-field to minimize the diffraction effects

The results of optical optimization indicated the importance of rigidly fixing the capillary flow cell If it is not rigidly fixed any mechanical vibration, for example, caused by the air flow around the capillary or e droplet exiting the capillary outlet, would affect both the fluorescence signal and background scatter

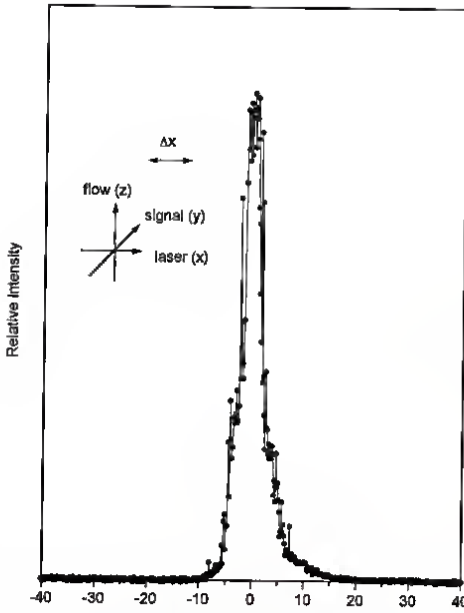

Figure 5-4 Effect of collecting microscope objective (MO1) on fluorescence

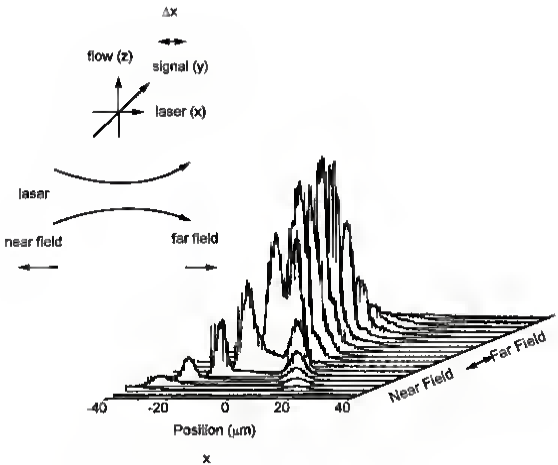

Figure 5-5 The fluorescence profile at different focus positions

Moreover mechanical vibrations may introduce a low frequency noise that can interfere with the analytical signal. A rigidly fixed capillary is especially important when the dimensions of the capillary inside diameter and the focused laser beam diameter are of the same size.

Evaluation of Analyte and Solvent

Several visible dyes, such as R-6G, phycoerythrin, have been chosen for single molecule detection. In the LIF-MVF system, the analyte has to be efficiently excited at 780.023 nm with high absorption coefficient, high fluorescence quantum efficiency, and a large Stokes shift. Very few chemicals fluoresce in the near-IR. The polymethine dyes are very attractive because they combine these characteristics in the near-IR. IR125, IR132, and IR140 are potentially useful for single molecule detection with excitation at 780.023 nm. By excitation at 780.023 nm, the wavelengths of maximum fluorescence for IR125, IR140, and IR132 are 806 nm, 833 nm, and 843 nm, respectively.[34]

In this project, a Rb MVF is applied to remove the laser specular scatter from the capillary. Any noise sources, such as the Raman scatter from the solvent and background fluorescence from the laser would significantly degrade the S/N ratio for single molecule detection. Lehotay has evaluated the Raman scatter from various solvents.[35] Water would be the ideal solvent due to its great applicability to many types of analytes. Unfortunately, IR132 and IR140 are not water-soluble and IR125 decomposes rapidly in water. Therefore, water is not a good choice as

a solvent in this project. Some other solvents, such as acetone and acetonitrile, also can not be used for single molecule detection due to the overlaps between Raman scatter from the solvent (820 nm) and fluorescence emission from molecules (800 nm to 850 nm). Methanol is the best solvent for near-IR single molecule detection due to the large Raman shift (860 nm) from the fluorescence peak.

The intensity of the emitted fluorescence should be maximized to optimize the LIF performance. Simultaneously, the amount of background noise should be minimized. Various band pass spectral filters are applied to further attenuate the background noises (see Table 4-5). The effects of different 10-nm band pass interference filters on the methanol blank are shown in Figure 5-6. A filter centered at 830 nm (s-10-830) gives the minimum blank signal. The higher background for other band pass filters is believed to be due to the long-tail laser background (s-10-810 and s-10-820) or Raman scatter (s-10-840 and s-10-850). This implies that the best S/N ratio would be obtained when the analyte dissolved in methanol has a maximum fluorescence peak at 830 nm. Figure 5-7 gives the measured S/N ratio for IR125, IR140, and IR132 dissolved in methanol with different band pass spectral filters. It is found that IR140 gave the maximum S/N ratio with a 10 nm band pass filter centered at 830 nm. Therefore, IR140 dissolved in methanol with a s-10-830 interference filter was used in this LIF-MVF system.

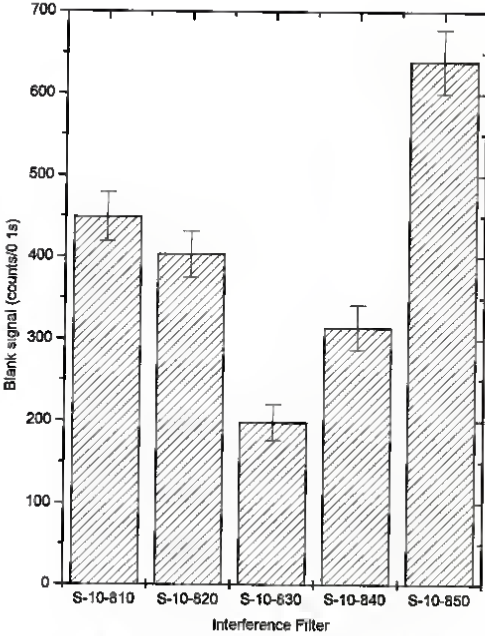

Figure 5-6 Effect of different band pass filters on blank.

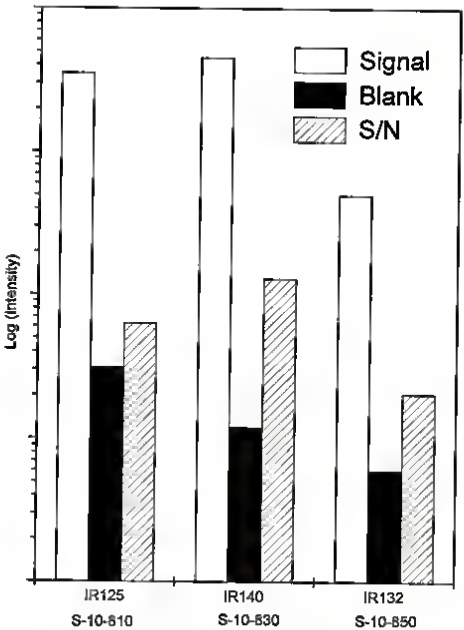

Figure 5-7 S/N for IR125, IR140, and IR132

Absorbance of Rb Metal Vapor Filter

Figure 5-8 shows the experimental set-up for absorbance measurements which is the same as LIF-MVF system for single molecule detection except the capillary is replaced with a high reflection mirror. A neutral density filter (optical density = 1.6) is placed before beam expander to attenuate the laser power. An interference filter (10-nm band pass centered at 780 nm) was used to block the stray light. Two sets of commercial neutral-density filters were calibrated at 780.023 nm to extend the dynamic range of the absorbance measurements. Figure 5-9 shows the measured absorbance for these neutral-density filters. The uncertainty for each neutral-density filter is usually less than 5%. The Rb MVF was sufficiently heated and the laser was tuned to the Rb transition line at 780.023 nm. The temperature of the Rb MVF could be controlled by adjusting the furnace temperature. The transmitted signal through the Rb MVF was then measured at different temperatures by the stacked neutral density filters. The measured transmittance was converted to absorbance at various temperatures. The results are shown in Figure 5-10, where the absorbance of the laser scatter is plotted as a function of temperature. The maximum absorbance of approximately 8 at 170 °C is believed to be limited by a weak, broad-band laser background fluorescence from the Ti:sapphire crystal.

Since the partial pressure of the Rb vapor phase is strongly dependent upon the temperature of the metal, the density of the metal vapor and thus the absorbance of MVF can be adjusted by varying the temperature of the MVF. In

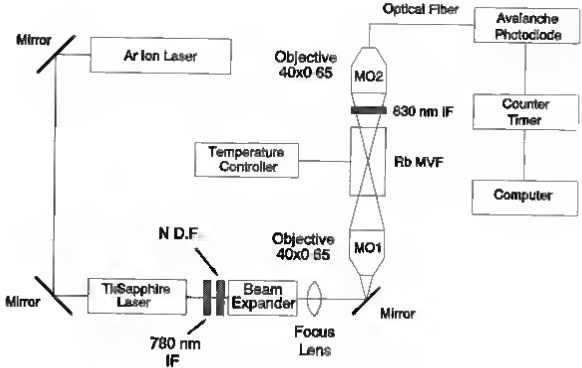

Figure 5-8 Experimental set-up for absorption measurement.

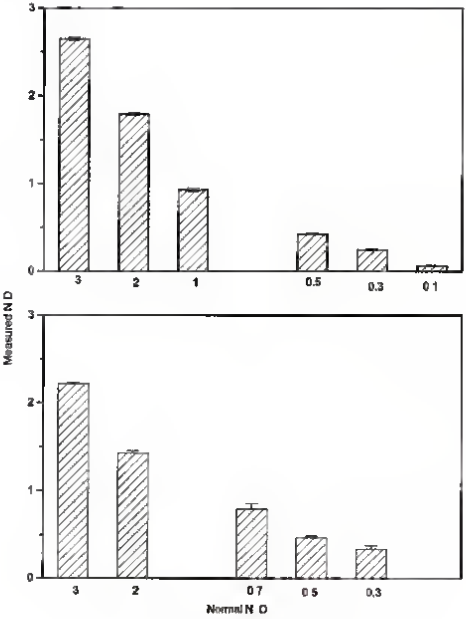

Figure 5-9 Calibration of neutral density filters

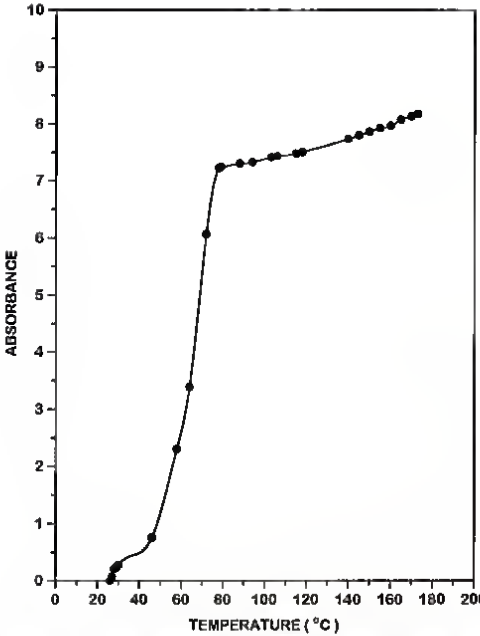

Figure 5-10 Measured absorbance of Rb MVF at different temperatures

addition to increasing the absorbance, raising the temperature of the MVF also broadens the width of the absorption peak, particularly if a buffer gas is used. Even if the line width of the laser is narrower than the absorption band width of MVF, the wing of laser lines experiences much less attenuation, and make up most of the transmitted light to the detector. Table 5-1 lists the experimental parameters used for the absorbance measurements. When the Rb MVF was at room temperature, the photon count rate corresponding to 80 mW laser power was approximately $4x10^{13}$ counts per second. When the Rb MVF temperature was 170 ^{0}C, the measured photon count rate was 1000 counts per second at 780.023 nm. Therefore, the absorbance of Rb MVF at 170 ^{0}C for 780.023 nm light is greater than 10. It is unclear how much greater the absorbance of Rb MVF really was, since most of the 1000 counts per second at 170 ^{0}C were due to laser background or stray light.

With the Rb MVF, we have looked at the wings of the Argon ion pumped Ti:sapphire laser nominally at 780.023 nm and found that there is indeed a background pedestal over 8 orders of magnitude below the laser peak intensity and extending to several nm around the laser output. Similar pedestals (modes) occur with diode lasers. Such pedestals (modes, wings), of course, limit the stray light rejection of the MVF to an absorbance A=8, with Ti:sapphire laser and Rb MVF. It is possible to improve the practical performance of the MVF by suitable design and optimization of the cavity of the Ti:sapphire laser that this background could be further reduced. Because the spectral profiles of either Ti:sapphire laser

Table 5-1 Experimental parameters used for absorbance measurements.

Laser Power (mW)	80 mW
Neutral Density Filter	1 80
Reflectance of Mirror	0 95
Collection Efficiency of MO1	0 10
Transmittance of MO1	0.90
Transmittance of Rb MVF	0 95
Transmittance of Interference Filter	0 80
Collection Efficiency of MO2	0.90
Transmittance of MO2	0 95
Transmittance of Optical Fiber	0.90
Detection Efficiency of Detector	0 25

or diode laser are not known accurately in the wings (the wings would have to be known accurately to better than 10^{-10} I_o, where I_o is the peak laser intensity), it is not possible to convolute the atomic absorption profiles of the MVFs with the laser spectral profiles

Estimation of Probe Volume

In order to estimate the probe volume within the capillary, knowledge of the focused laser beam diameter as well as the capillary inside diameter is required. The beam diameter was measured by translating a razor blade through the laser beam using a microtranslational stage and the laser power was monitored with a photodiode. Figure 5-11 shows the laser beam diameter near the focus. The minimum $1/e^2$ beam intensity is determined to be 11 μm. Figure 5-12 is the beam intensity profile of the laser beam diameter at focal point. A theoretical Gaussian intensity profile shows good agreement when fitted to the measured beam intensity profile. The probe volume formed by the capillary and the focused laser beam is estimated to be approximately 1.05 picoliter.

Estimation of Transit Time

The average flow velocity can be estimated from the volumetric flow rate and the cross section area of the capillary (Θ 5×10^{-7} cm^2). The average molecular transit time through the probe volume can be simply determined using the equation

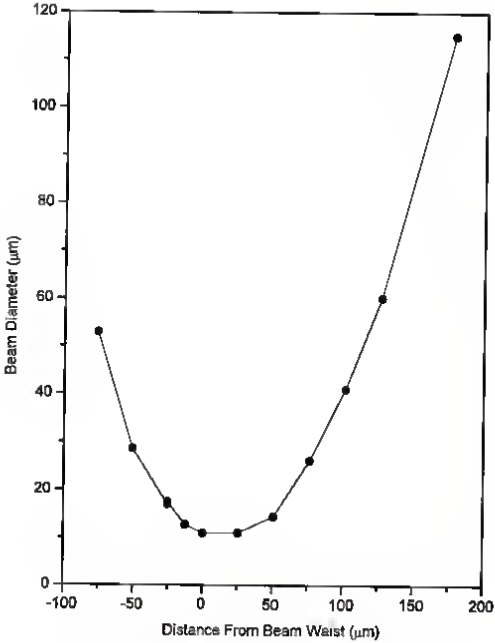

Figure 5-11 Laser beam diameter near the focus

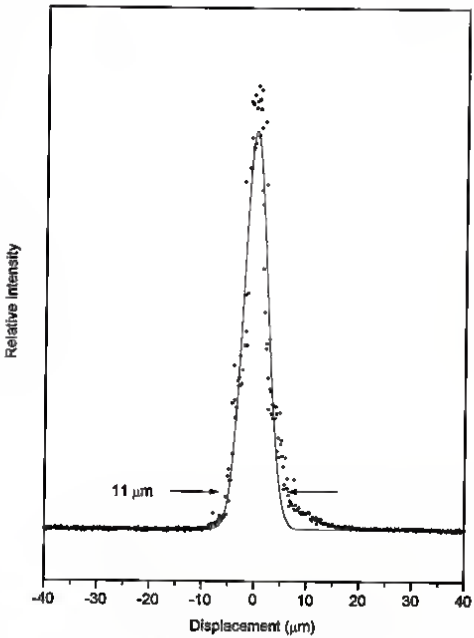

Figure 5-12 Measured laser beam diameter at the focus

$$Transit\ time = \frac{Diameter\ of\ laser\ beam}{Average\ flow\ velocity} \qquad (5\text{-}1)$$

The calculated transit time is approximately 1 ms for a capillary with 11-μm inside diameter when the volumetric flow rate of syringe pump is set at 0.061 μL/min. Possible deviations from the actual molecular transit time in the probe volume are the uncertainties of the small capillary inside diameter, distorted laser beam shape within the cylindrical capillary, and Brownian diffusion.

Effect of Transit Time and Laser Power

A study of the emitted fluorescence intensity as a function of the flow velocity allowed the determination of the influence of photodestruction. The quantum yield of photodestruction Q_d can be determined by measuring the dependence of the normalized fluorescence intensity S' on the flow velocity v of molecules passing through the probe volume. Figure 5-13 shows the degree of photodestruction of IR140 at different flow velocities within a capillary flow cell (11-μm inner diameter). The dots denote the measured values, and the solid curve is the best fit of equation (2-22) obtained for $Q_d = 2.5 \times 10^{-6}$. This value is somewhat lower than those highly fluorescent molecules, e.g., fluorescein ($Q_d = 2.7 \times 10^{-5}$) and phycoerythrin ($Q_d = 1.1 \times 10^{-5}$), which leads to the conclusion that IR140 dissolved in methanol is less photolabile. The fluorescence intensity decreased from 80% to 15% of its maximum value when the flow was slowed from 1.07 cm/sec to 0.053

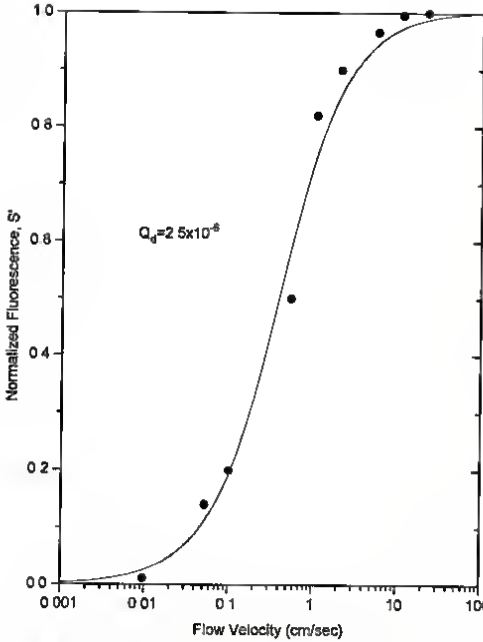

Figure 5-13 Measured photodestruction curve for IR140 in methanol

cm/sec. The time spent by a fluorescent molecule in the illuminated volume increased from 1 msec to 20 msec over this range, which increased its probability of being photodestructed. This implies that when the flow velocity is 1.07 cm/sec, approximately 15% of IR140 molecules are affected by photodestruction. Because of the limitation of the counter/timer board (minimum integration time = 200 μs), the flow velocity (1.07 cm/sec) for a 1 ms transit time was used for single molecule detection.

A plot of fluorescence signal versus laser power for [IR140] = 6.4x10^{-10} M at a flow rate of 1.07 cm/sec is shown in Figure 5-14. The fluorescence signal is linear with laser power up to about 50 mW, above 50 mW, there is less than linear increase of fluorescence signal with laser power. The curvature is most likely a convolution of optical saturation and photodestruction effect. The variation of S/N ratio with laser power has been discussed by Mathies et al [49]

Analytical Calibration Curve

Figure 5-15 shows a log-log plot of the monitored IR140 fluorescence emission versus the sample concentration within the 11-μm-inner-diameter capillary flow cell. These calibration curves were examined over the concentration range from 1.5x10^{-13} M to 1.5x10^{-9} M at 3 different laser powers while the molecular transit time in the probed volume was 1 ms. The fluorescence signal had good linearity for at least 4 orders of magnitude from 1.5x10^{-12} M to 1.5x10^{-8} M. Within this linear concentration range, the average number of molecules

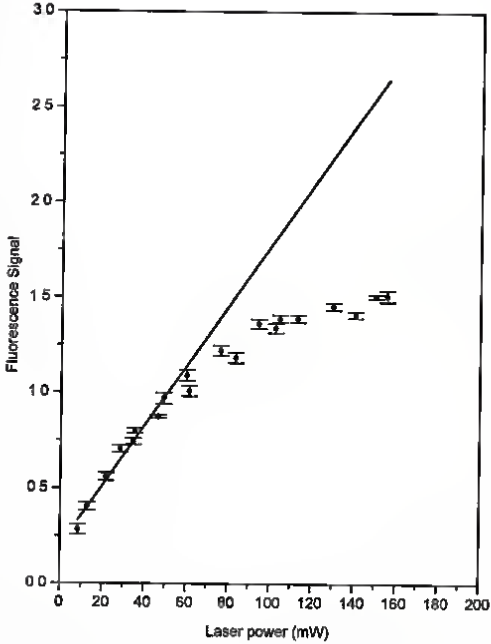

Figure 5-14 Fluorescence signal of IR140 (6.4x10^{-10} M) at various laser powers

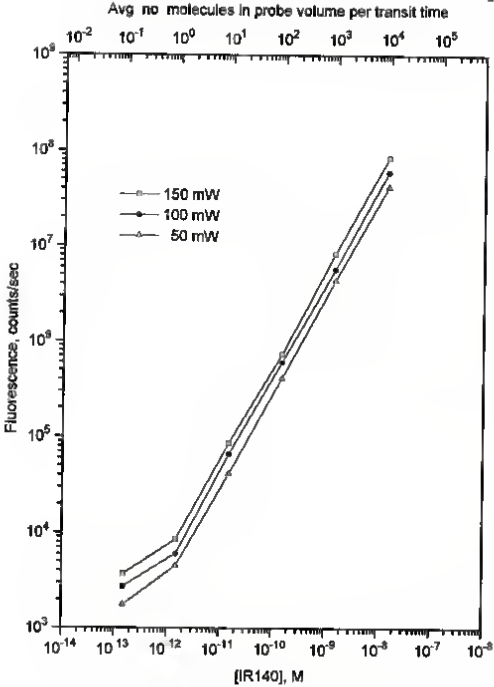

Figure 5-15 Calibration curve of IR140 for different laser powers

present in the probe volume per transit time were from 1 to 10000. Since the transit time is 1 ms, then the number of molecules that actually travel through the probe volume at a concentration of $1.5x10^{-13}$ M is approximately 1000 in this 1 sec integration time. At $[IR140] = 1.5x10^{-13}$ M, since there is only a 10% probability of finding a molecule in the 1.05 pL probe volume at 1 ms transit time, approximately 100 IR140 molecules would actually pass through the probed volume during the 1 sec integration time.

Single Molecule Detection

Poisson Distribution

When an experiment is carried out in which the analyte is present at a very low level then the appearance of the number of molecules in the probe volume at any instant may follow a Poisson distribution. The Poisson distribution is a discrete probability distribution that follows the general formula

$$P(X) = \frac{\mu^X e^{-\mu}}{X!} \qquad (5\text{-}2)$$

where

P(X) = the probability of X events occurring

μ = the mean value of X.

For a Poisson distribution, the mean value μ of X is also the variance of the distribution of X. In practice, the Poisson distribution has been useful in finding the

probability of X occurrences of an event that occur randomly over an interval of time, provided certain assumptions are met.

(1)Events occur one at a time, two or more events do not occur precisely at the same time.

(2)The occurrence of an event in a given period is independent of the occurrence of the event in a non-overlapping period, that is, the occurrence (or nonoccurrence) of an event during one period does not change the probability of an event occurring in some later period

Figure 5-16 shows the calculated Poisson distribution using equation (5-2) with different mean value μ. Note the different shapes of Poisson distributions at different mean values (μ). For $1 \geq \mu > 1$, the maximum number of occurrences is when $X = 1$. For $\mu = 1$, $X = 0$ and $X = 1$ have the same maximum number of occurrences. For $\mu < 1$, the maximum number of occurrences shifts from $X = 1$ to $X = 0$

Occupancy of Molecules in Probe Volume

To assure that only one molecule resides within the probe volume at any given time, the probability of two or more than two molecules occupying the probe volume must be minimized. Assume the number of molecules in the probe volume during the transit time follows the Poisson distribution. The probability that n molecules occupy the probe volume simultaneously is given by

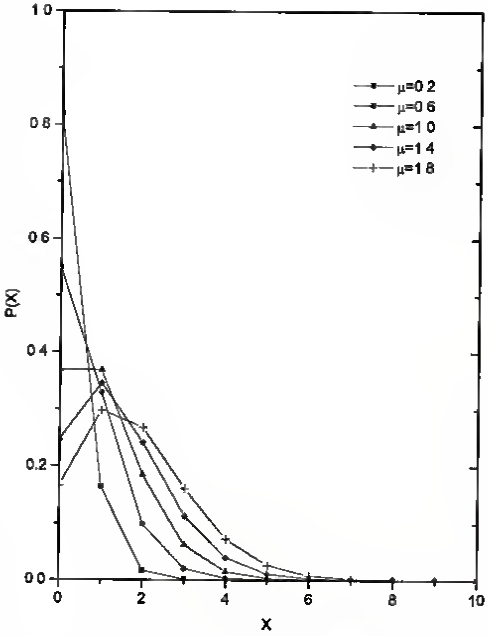

Figure 5-16 Poisson distribution at different mean (μ)

$$P\left(N_{t+m} - N_t = n\right) = \frac{(\lambda_v m)^n e^{\lambda_v m}}{n!} \qquad (5\text{-}3)$$

where

N_t = number of molecules arrived at time t.

λ_v = average number of molecules in probe volume per time segment.

m = number of time segments per transit time

At [IR140] = 1.5×10^{-12} M, the average number of molecules in the probe volume (1.05 pL) is 0.1. Therefore $\lambda_v = 0.02$ and m = 5 for 1 ms transit time and 200 μs time segment. Table 5-2 gives the probability (estimated from equation (5-3)) for different numbers of molecules occupying the probe volume at any given time. Most of time, there is no molecule in the probe volume (P(n=0) = 0.905). The probability of one molecule occupying the probe volume is P(n=1)=0.090 while the probability of multiple occupancy ($P(n \geq 2)$=0.005) is relatively low and can be neglected.

Model for the Arrival of Single Molecules

For single molecule detection (if the solution is well mixed and the flow rate is constant), the number of molecules (N_p) in the probe volume during the transit time will be assumed to follow a Poisson distribution. The assumption of a Poisson distribution of N_p is considered valid in low-level experiments if the

Table 5-2 The probability for different numbers of molecules occupying the probe volume at any given time ([IR140] = 1.5×10^{-13} M, probe volume = 1.05 pL)

No. Molecules in Probe Volume	Probability
0	0.905
1	0.090
2	0.005
3	0.000

appearance of a molecule in the probe volume is due to a random process. In addition, the distribution in the number of signal counts (in this case, number of photoelectrons from single molecules) detected during the transit time will generally follow the Poisson distribution because of the nature of the distribution of N_s. The observed number of signal counts X(t) at time unit t is given by

$$X(t) = Z(t) + B(t) \tag{5-4}$$

if A(t) + A(t-1) + ... + A(t-m-1)≥1 (at least one molecule in one of time segments) or

$$X(t) = B(t) \tag{5-5}$$

if A(t) + A(t-1) + ... + A(t-m-1) = 0 (no molecule in any time segment)

where

Z(t) = signal counts from analyte

B(t) = signal counts from blank

A(t) = $N_t - N_{t-1}$

(number of molecules arrived for every time segment)

Assume signal counts emitted from analyte (Z(t)) and blank (B(t)) are two independent processes and both follow the Poisson distribution. Hence the observed probability to detect n signal counts, $P(X_t=n)$, is given by

$$P(X_t = n) = \Gamma P(B_t = n) + (1 - \Gamma) P(Z_t + B_t = n) \tag{5-6}$$

where

$P(X_t=n)$ = probability to detect n signal counts from IR140 raw data at time t.

$P(B_t=n)$ = probability to detect n signal counts from methanol raw data at time t.

$P(Z_t+B_t=n)$ = probability to detect n signal counts from both IR140 and methanol at time t.

Γ = proportional constant (to be evaluated).

Equation (5-6) can be rewritten as

$$\frac{\lambda_x^n e^{\lambda_x}}{n!} = \Gamma \frac{\lambda_s^n e^{-\lambda_s}}{n!} + (1-\Gamma) \frac{(\lambda_z+\lambda_s)^n e^{(\lambda_z+\lambda_s)}}{n!} \qquad (5\text{-}7)$$

where

λ_x = average signal counts per time segment in IR140 raw data.

λ_s = average signal counts per time segment in methanol raw data.

λ_z = average signal counts per time segment in analyte (to be evaluated)

Since λ_x and λ_s can be obtained from the IR140 and methanol raw data, hence λ_z and Γ can be estimated by solving the non-linear equation for $n = 0$ and $n = 1$

Counting the Molecules

The typical experimental parameters for single molecule detection are given

In Table 5-3. Figure 5-17 and Figure 5-18 show the raw data for the blank (methanol) and IR140 (1.5×10^{-13} M) when excited at 50 mW, 100 mW, and 150 mW laser powers. At [IR140] = 1.5×10^{-13} M, the average number of molecules in the probe volume at any time is 0.1. There is a clear difference between the IR140 and the blank raw data. The number of photoelectron counts collected in each 200-μs segment is displayed within a total of 200 ms measurement time. The sample flow velocity is reduced to 0.061 μL/min so that it takes approximately 1 ms for a single IR140 molecule to transit the laser beam. Therefore, during a single analytical run of 200 ms, 20 molecules on the average should pass through the probe volume. Table 5-4 summarizes the average number of photoelectron signal counts per 200 μs segment for the blank and IR140 molecules at different laser powers.

The observed and fitted signal counts using equation (5-7) are summarized in Table 5-5. A comparison of observed and fitted signal counts for IR140 and methanol are shown in Figure 5-19 and Figure 5-20, respectively. The goodness of fit implies that the noise in the detection process is limited by photon statistics (Poisson distribution). A histogram of signal counts from [IR140] = 1.5×10^{-13} M and the blank at different laser powers is shown in Figure 5-21. Note that there are many more high signal counts in the IR140 raw data than in the blank. However, it is difficult to identify and isolate the photon bursts from individual single molecules due to the large overlap of signal counts between IR140 and blank. Nevertheless, each of the high signal counts ($\geq$ 3 counts) in the IR140 raw data

Table 5-3 Experimental parameters used for single molecule detection.

Dye	[IR140] = 1.5×10^{-13} M
Solvent	Methanol
Rb MVF bandwidth	21 pm
Rb MVF absorbance	8
Laser wavelength	780.023 nm
Laser linewidth	< 0.061 pm
Laser power	50 mW, 100 mW, 125 mW
Laser beam diameter	11 μm
Capillary	11 μm ID x 140 μm OD
Probe volume	1.05 pL
Flow rate	0.061 μL/min
Transit time	1 ms

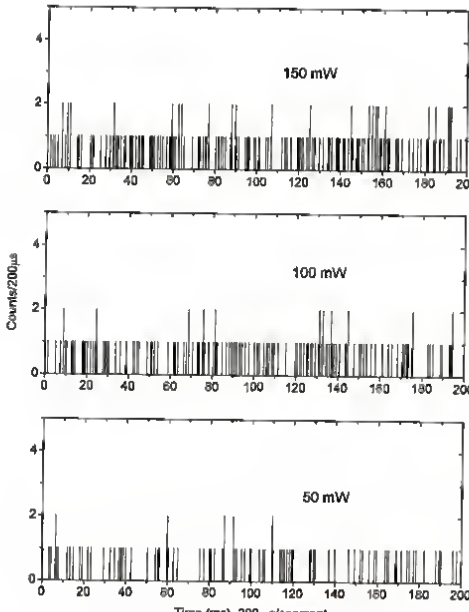

Figure 5-17 Raw data for methanol at different laser powers

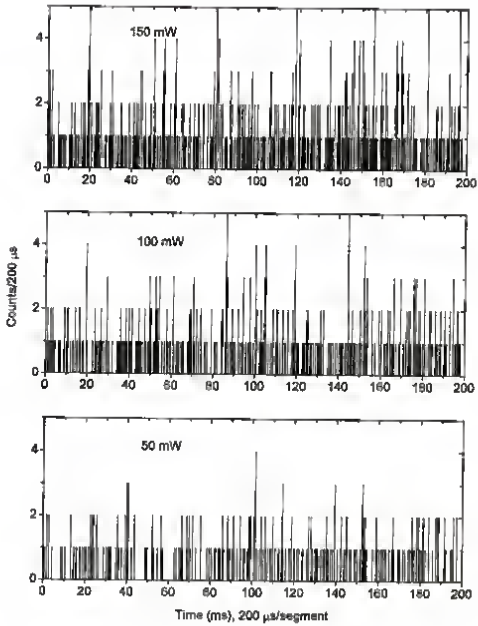

Figure 5-18 Raw data for IR140 at different laser powers.

Table 5-4 The average signal counts per time segment from IR140 and blank.

	Average signal counts per time segment		
	50 mW	100 mW	150 mW
Blank	0.101	0.176	0.218
IR140	0.327	0.526	0.701

Table 5-5 Observed and fitted probability distribution for methanol and IR140 at different laser powers.

	150 mW		100 mW		50 mW	
λ_1	0.219		0.176		0.101	
λ_2	0.666		0.462		0.482	
r	0.31		0.27		0.53	
Methanol	Obs	Fit.	Obs.	Fit.	Obs	Fit.
n=0	799 (0.806)	797 (0.804)	828 (0.836)	831 (0.839)	896 (0.904)	896 (0.904)
n=1	168 (0.170)	173 (0.175)	152 (0.153)	147 (0.148)	90 (0.091)	90 (0.091)
n=2	24 (0.024)	19 (0.019)	11 (0.011)	13 (0.013)	5 (0.005)	5 (0.005)
n ≥ 3	0 (0.000)	2 (0.002)	0 (0.000)	0 (0.000)	0 (0.000)	0 (0.000)
IR140	Obs	Fit.	Obs	Fit.	Obs	Fit.
n=0	530 (0.535)	529 (0.534)	606 (0.612)	606 (0.612)	732 (0.739)	733 (0.740)
n=1	303 (0.306)	303 (0.306)	283 (0.286)	283 (0.286)	201 (0.203)	200 (0.202)
n=2	111 (0.112)	116 (0.117)	77 (0.078)	61 (0.062)	52 (0.052)	47 (0.047)
n=3	28 (0.026)	33 (0.033)	18 (0.018)	17 (0.017)	5 (0.005)	9 (0.000)
n=4	11 (0.011)	7 (0.007)	5 (0.005)	3 (0.003)	1 (0.001)	1 (0.001)
n ≥ 5	8 (0.008)	3 (0.003)	2 (0.002)	0 (0.000)	0 (0.000)	1 (0.001)

* Number in parentheses is the probability

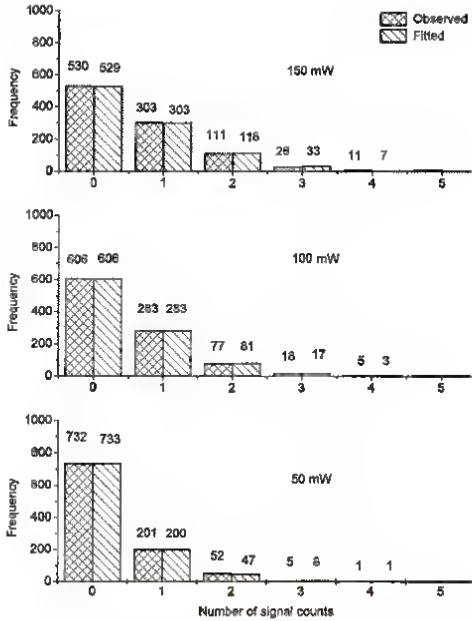

Figure 5-19 Observed and fitted signal counts for IR140

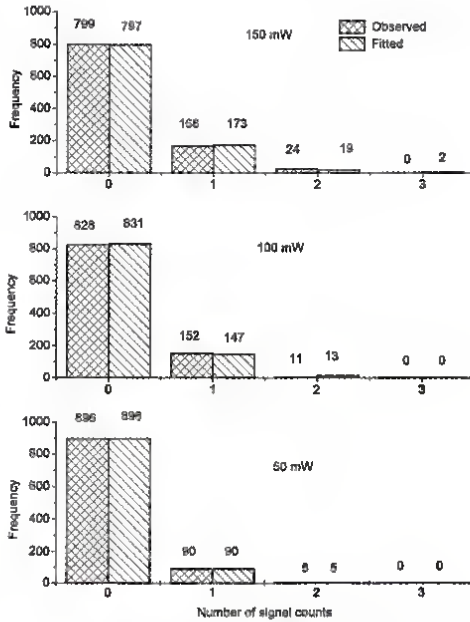

Figure 5-20 Observed and fitted signal counts for methanol

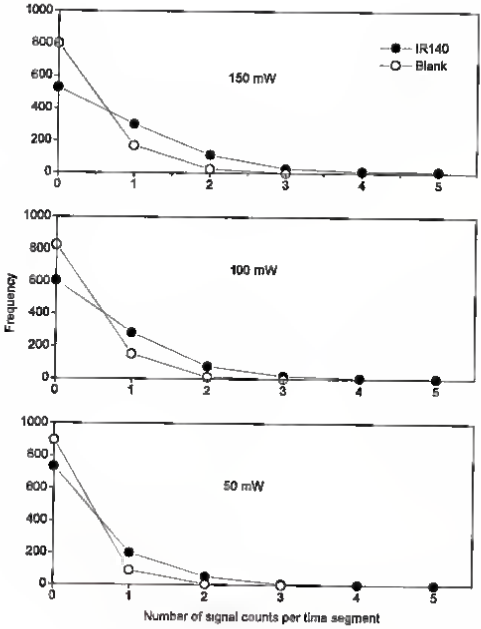

Figure 5-21 Histograms (raw data) for IR140 and blank.

does indeed represent a single molecule (see Figure 5-16).

It is possible to estimate the average number of events expected as single IR140 molecules transit through the focused laser beam. Here, the number of events is the number of time segments with any signal counts from IR140. The number of events, N_{ev}, for all molecules traveling through the probe volume during the measurement time T can be estimated from

$$N_{ev} = \frac{N_p T m}{\tau_t} \tag{5-6}$$

where

N_{ev} = number of events from single molecules during the measurement time

N_p = average number of molecules in probe volume

τ_t = transit time of single molecules in probe volume

m = number of time segment per transit time

For a typical experimental run (N_p=0.1, T=200 ms, m=5, and τ_t=1 ms), the calculated total number of events N_{ev} is 100.

To obtain the photon bursts from individual single molecules, various signal processing methods have been proposed for the continuous detection and monitoring of molecules entering the probe volume.[16,17,19,20,46,47,58] The individual photon bursts are analyzed and searched within the data stream in order to obtain direct evidence for single molecule sensitivity. To enhance the visibility of photon

bursts from single molecules, the weighted quadratic summing (WQS) filter, a modified sliding sum method, has been evaluated and demonstrated to be an efficient photon burst indicator of a passing single molecule in previous single molecule detection experiments. The raw data is squared and processed with the WQS filter algorithm, which is given by

$$S(t) = \sum_{\tau=1}^{m-1} w(\tau)\, d^2(t+\tau) \qquad (5\text{-}9)$$

where m covers time intervals which are approximately equal to the transit time of a single molecule through the probe volume, $w(\tau)$ is a weighted factor, and $d(t+\tau)$ is the raw data point at time $t+\tau$. As the molecules cross the laser beam, the fluorescence signal increases slowly, followed by an abrupt cessation, when the molecule is photodecomposed. To best discriminate the time-correlated fluorescence signal from the random background noise, the weighing factor, $w(\tau)$, is chosen as an asymmetric triangular ramp,

$$w(\tau) = \frac{(\tau+1)}{m} \qquad (5\text{-}10)$$

In the present experimental system, since the average transit time of IR140 molecules in the probe volume is 1 ms, m is set to 5 for a counter with 200 μs time segment.

Figure 5-22 and Figure 5-23 show the WQS filtered data for [IR140] = 1.5

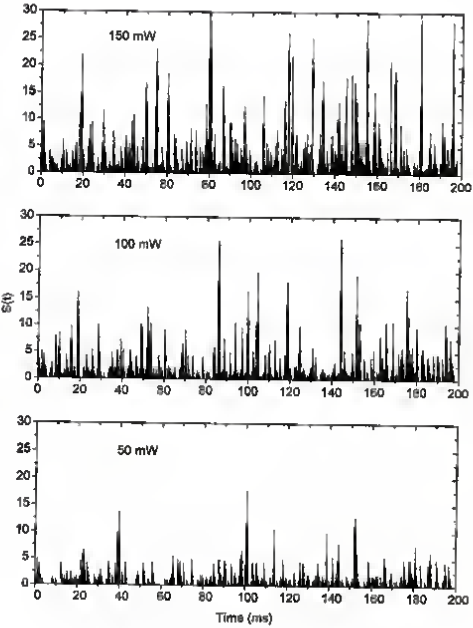

Figure 5-22 WQS data for IR140 at different laser powers.

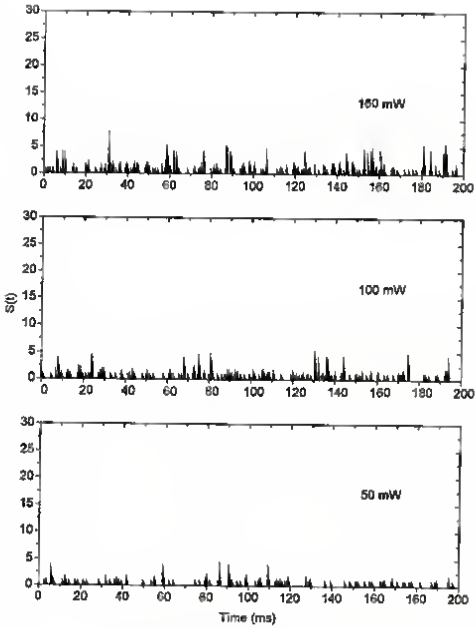

Figure 5-23 WQS data for methanol at different laser powers

x 10^{-13} M solution and methanol blank, respectively. Within the 200 ms sampling time, approximately 20 molecules pass through the probe volume. The large amplitude bursts from the IR140 solution are clearly evident for single molecules passing through the center of laser beam. The variation in the burst amplitude arises from the molecules flowing through different parts of the Gaussian intensity laser profile. When the molecules travel through the edges of the laser beam, they experience fewer excitation cycles and thus emit fewer fluorescence photons. Variations in the solvent blank photoelectron bursts are due to fluctuations of background and dark counts.

In order to evaluate the detection efficiency for the near-IR dye molecules, a plot of the cumulative number of WQS filtered events exceeding a discriminator threshold is constructed for the solvent blank and the dye solution. Figure 5-24, Figure 5-25, and Figure 5-26 show the results of this analysis when excited at 50 mW, 100 mW, and 150 mW laser powers, respectively. Since the spatial probing efficiency is near 100%, the measurement efficiency is defined as the ratio of measured to expected total number of events for molecules flowing through the capillary. To minimize the false positive probability from the blank, the discriminator threshold is set at S(t) = 4, 6, and 9 for 50 mW, 100 mW, and 150 mW laser powers, respectively. The number of events that exceed the threshold for the IR140 molecules is found to be 105, 107, and 109 within this laser power range, while less than 1 event is due to blank. Since the expected number of events during this 200 ms sampling time is approximately 100 (see equation (5-8)), the

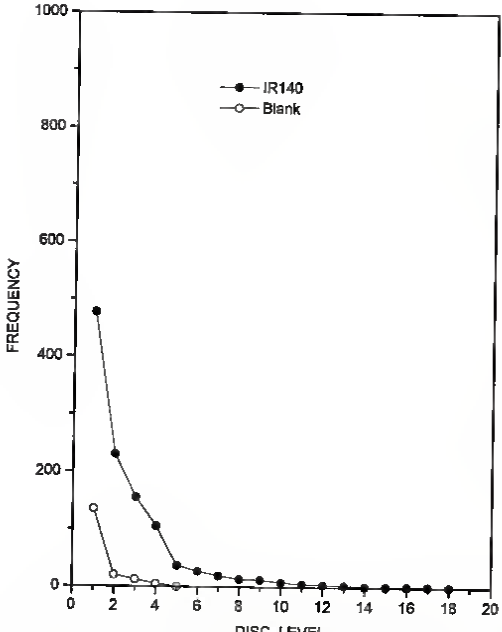

Figure 5-24 Histogram (WQS) of IR140 and methanol at 50 mW laser power

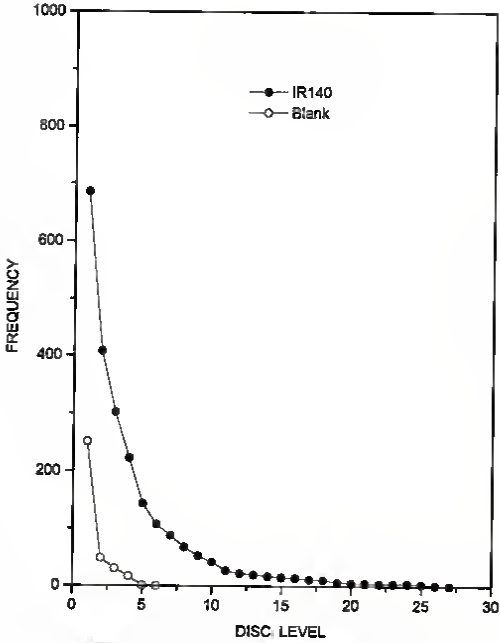

Figure 5-25 Histogram (WQS) of IR140 and methanol at 100 mW laser power

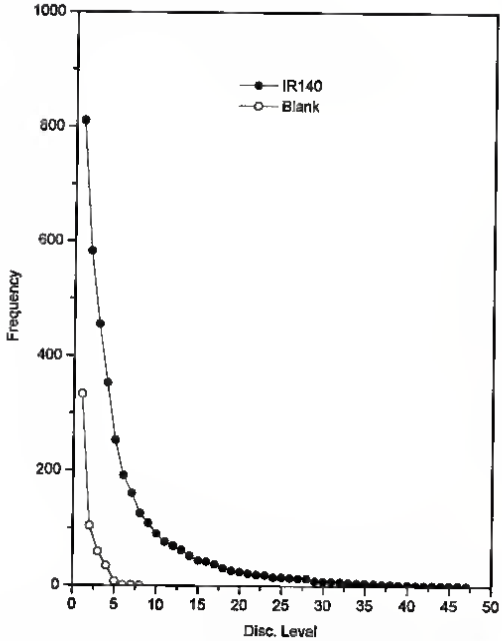

Figure 5-26 Histogram (WQS) of IR140 and methanol at 150 mW laser power

detection efficiency is calculated to be slightly above 100%, which is believed to be due to errors in the estimation of analyte concentration and the probe volume. Table 5-6 summarizes the total number of measured and expected events from a single molecule with excitation at different laser powers. A higher discriminator threshold is required when the laser power is increased while maintaining similar detection efficiency. To designate photon bursts from single molecules, the raw data stream is compared with WQS filtered data. The corresponding raw data points with WQS amplitude higher than the specific discriminator threshold are binned to five (200 μs x 5) within the 200 ms sampling time. To locate the photon bursts from single molecules, Figure 5-27, Figure 5-28, and Figure 5-29 show the raw data as well as WQS filtered data for [IR140] = 1.5×10^{-13} M for laser powers of 50 mW, 100 mW, and 150 mW. Positions of five consecutive time segments with large sums of events are indicated as *. The average number of photoelectrons detected from a single IR140 molecule while traveling through the probe volume per transit time are 9.1, 6.6, and 5.4 for 150 mW, 100 mW, and 50 mW laser power, respectively (see Table 5-6). An expanded plot for IR140 raw data at 150 mW laser power is shown in Figure 5-30. When a molecule passes through the laser beam, the distribution in time of the segment counts should mirror the Gaussian profile of the laser beam. However, for low photoelectron counts, Poisson noise severely distorts the Gaussian nature of the distribution. An additional complication in this experimental arrangement is that some of the molecules pass near the edge of the focused laser beam. This affects the

Table 5-6 Number of events from a single molecule at different laser power

laser power	50 mW	100 mW	150 mW
discriminator	4	6	9
measured events	105	107	109
expected events	100	100	100
av photoelectrons per molecule*	5.4	8.6	9.1

* Average number of photoelectrons per molecule is calculated as $(\Sigma C_i) / N$, where N is the number of molecules with WQS amplitude higher than the discriminator level and C_i is the photon counts from an individual molecule using the raw data.

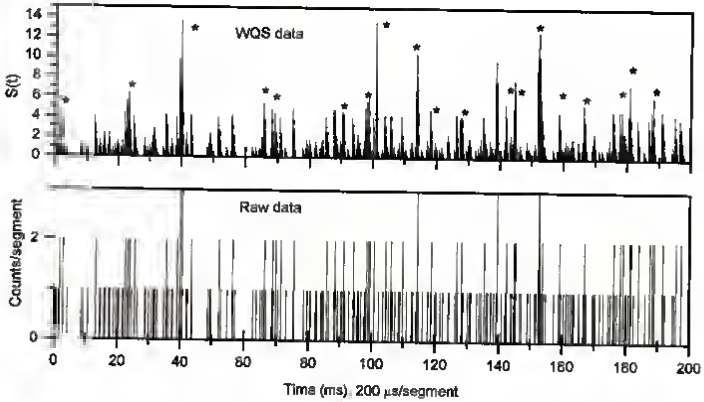

Figure 5-27 Copmparison of WQS and raw data for IR140 at 50 mW laser power

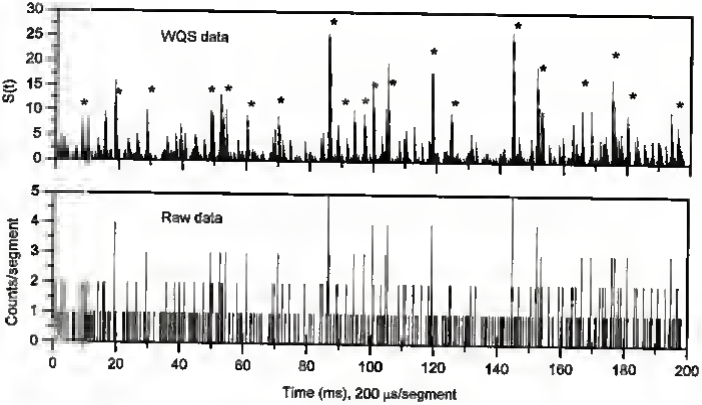

Figure 5-28 Comparison of WQS and raw data for IR140 at 100 mW laser power

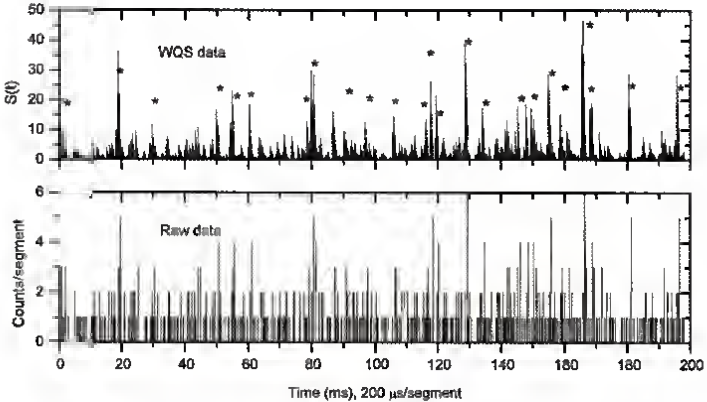

Figure 5-29 Comparison of WQS and raw data for IR140 at 150 mW laser power

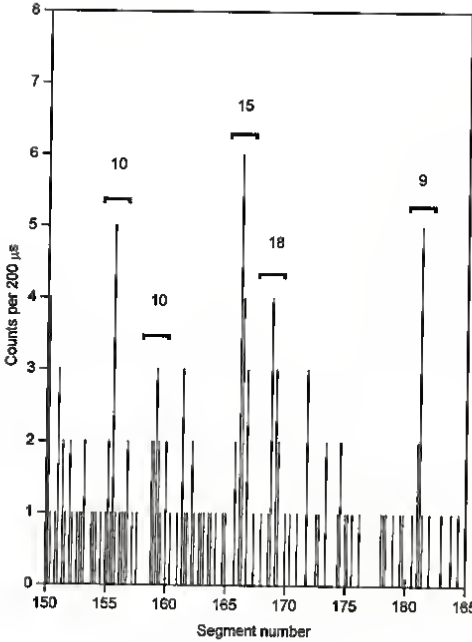

Figure 5-30 Expanded raw data for IR140 at 150 mW laser power

histogram and makes the exact counting of the molecules more difficult. Since the average background counts per transit time is ≤ 1 count, 5 or more signal counts justifies the use of the limit of detection (LOD) concept, but does not justify the case of the limit of guarantee (LOG), as discussed in Chapter 2.

Table 5-7 summaries the results for the visible single molecule detection (R-6G[17]) and the near-IR single molecule detection (IR132[18] and IR140). When compared with visible R-6G molecules, the excitation and observation wavelengths have been shifted by approximately 300 nm into the near-IR region of the spectrum. The principle advantage of the large shift into the near-IR is a significant reduction in the fluorescence from impurities in the background due to the fact that these impurities demonstrate negligible excitation cross sections in the near-IR. The result is a lower discriminator threshold and a higher single molecule detection efficiency.

Although the average photon yield per molecule is lower for IR140 with similar photon detection efficiency as compared to IR132, the measurement efficiency is two orders of magnitude higher because the whole capillary inside diameter is fully illuminated with the laser beam to assure near 100% spatial probing efficiency.

Table 5-7 Comparison of single molecule detection for R-6G, IR132, and IR140

parameter	R-6G [a]	IR132 [b]	IR140 [c]
excitation wavelength (nm)	532	800	780
observe wavelength (nm) [d]	570 (40)	840 (30)	830 (10)
photon detection efficiency	0 0007	0 007	0.007
probe volume (pL)	1 1	0 3	1
transit time (ms)	24	10	1
av photoelectron per molecule	39	18	9 1 [e]
detection efficiency	0 78	0 97	1
spatial probing efficiency	< 0 0001	0 01	1
measurement efficiency	<0 000078	0 0097	1

a. Data taken from reference 3.

b. Data taken from reference 33.

c This work.

d The number in parenthesis is spectral bandpass

e Laser power = 150 mW

CHAPTER 6
CONCLUSIONS AND FUTURE WORK

Conclusions

In summary, this work has demonstrated the photon burst detection of a single near-IR molecule (IR140) with high efficiency. There are several components that are interesting and relevant in the area of single molecule detection. For example, the use of the metal vapor filter and the high sampling efficiency produced by irradiating the entire internal diameter of the capillary tube are unique. A rubidium metal vapor filter has been shown to be successful in rejecting laser specular scatter from the capillary. The generalized Lorentzian approximation for the Voigt spectral line shape is applied to simulate the absorption profile of the rubidium metal vapor filter at different temperatures. The measured absorbance of the rubidium metal vapor filter at 170 °C is determined to be 8. The maximum absorbance is believed to be limited by the background fluorescence from the Ti:sapphire laser. The use of near-IR excitation and detection will benefit the ultrasensitive fluorescence detection due to reduced background noise sources from impurities. When compared with the molecules absorbing in the visible region, IR140 dissolved in methanol is less photolabile due to the lower photodestruction quantum efficiency ($Q_d = 2.5 \times 10^{-6}$). The sample flow is confined

in a fused silica capillary with 11-μm inner diameter. In order to have a 100% spatial probing efficiency, the capillary is irradiated with the focused laser beam (diameter=11 μm). The probe volume within the capillary is estimated to be 1.05 pL. The fluorescence signal has good linearity for at least 4 orders of magnitude from 1.5×10^{-12} M to 1.5×10^{-8} M. A mathematical model based on the Poisson distribution has been successfully applied to describe the events (photoelectrons) coming from single molecules. To enhance the detection of single molecules, a digital weighted quadratic summing filter is applied to extract the individual photon bursts from the raw data. By setting the discriminator threshold to minimize the false positive probability, the average number of signal counts detected from a single IR140 molecule are 5.4, 6.6, and 9.1 for laser powers of 50 mW, 100 mW, and 150 mW, respectively. Since the average background count per transit time is less than 1, a signal count of greater than 5 justifies the concept of LOD=1 molecule, but does not justify the case of LOQ=1 molecule.

Future Work

Preliminary results in this dissertation have indicated the capability of single molecule detection by laser-induced fluorescence/metal vapor filter configuration. The direction of future studies should be toward the evaluation of excitation sources, new near-IR fluorescent molecules, metal vapor filters, detection systems, data analysis, as well as practical applications.

The argon ion-pumped Ti:sapphire laser is expensive for the laser-induced

fluorescence experiments A commercial diode laser with 1 to 10 mW laser power will have a narrow line width of < 100 kHz in a 1 ms time period and < 5 MHz in a 5 sec time period with stability within 0 003 cm^{-1} and coarse tuning over a 10 - 20 nm range In addition to being compact, economic, stable, simple, and long-lived, a diode laser should be considered as the ideal excitation source for single molecule detection

To be used as a fluorescence probe for biologically important molecules, different near-IR dyes must be evaluated Especially, studies should be emphasized for those dyes which absorb at wavelengths ≥ 670 nm, with high fluorescence quantum efficiency, with good solubility in aqueous or near aqueous solutions, and with functional groups, like NH_2, which are suitable for derivatization with NCS groups

Because of the role in rejecting laser specular scatter, the metal vapor filter must be justified through an evaluation of the theoretical absorption spectral profile and experimental transmission measurements for different applications Since this work involves the use of near-IR dyes, it will be interesting to consider other atomic species elements with strong resonance transitions in the 670 nm - 1000 nm range.

With the present system, a single photon avalanche photodiode was used for single molecule detection. Unfortunately, this detector has a 50 ns dead time, which means that, after a photon is detected, the detector will not detect incoming photons until recovery from the breakdown. The dead time will limit the maximum

photon counting rate and cause the single photon avalanche photodiode to miscount the photons from the single molecules. So it is important to find a detector with a shorter dead time for photon counting experiments. In one task, using the PMT as the detector, the S/N ratio improved at least 3-fold even though the electronic device had a 2-ms dwell time between each sampling point. Therefore the performance of the PMT and the single photon avalanche photodiode should be evaluated for single molecule detection.

Because the single photon avalanche photodiode has a very small active area with diameter=50 μm, a microscope objective (NA=0.85) currently focused the fluorescence from capillary onto a optical fiber (NA=0.29) which was prealigned to the detector. The coupling in numerical apertures between microscope objective and optical fiber becomes another issue for S/N ratio optimization for single molecule detection. Since the collected photon flux is proportional to the square of the numerical aperture, approximately a 5-fold loss in signal is possible due to the miscoupling in the numerical aperture. Therefore, an optical fiber with large numerical aperture, similar to that of microscope objective, will also increase the signal counts for single molecule detection.

If the signal-to-noise ratio is high, the photon bursts from individual single molecules should be easily identified. However, a statistical model is required for data analysis when the size of photon burst is small as in this work. A model based on the Poisson distribution provides good agreement between the experimental and the theoretical results. How to locate every single molecule as

it passes through the probe volume becomes the other important issue for single molecule detection. Therefore, a sophisticated model is essential to simulate the events coming from the arrival of single molecules.

Finally, as mentioned in Chapter 1, there will be several practical applications for single molecule detection in the capillary flow cell. Coupled with the ultrasensitive detection apparatus and the near-IR excitation, it should be possible to apply near-IR single molecule detection to several different areas where ultrasensitive detection is critical, for example, DNA sequencing, flow cytometry, immunoassay, and any miniaturized chemical separation techniques involving capillary zone electrophoresis, open tubular capillary liquid chromatography, and packed capillary liquid chromatography.

REFERENCE LIST

1. G. S. Hurst, M. H. Neyfen, and J. P. Young, *Appl. Phys. Lett.*, **30**, 299 (1977)

2. C. L. Pan, J. V. Prodan, W. M. Fairbank, and C. Y. She, *Opt.Lett.*, **5**, 459 (1980)

3. W. E. Moerner and L.Kador, *Anal. Chem.*, **61**, 2171A (1989)

4. M. Orrit and J. Bernard, *Phys. Rev. Lett.*, **66**, 13762 (1991)

5. E. Betzig and R. J. Chichester, *Science*, **262**, 1422 (1993)

6. T. Hirschfeld, *Appl. Opt.*, **16**, 2965 (1976)

7. N. J. Dovichi, J. C. Martin, J. H. Jett, M. Trkula, and R. A. Keller, *Anal. Chem.*, **56**, 348 (1984)

8. B. Kirsch, E. Voigtman, and J. D. Winefordner, *Anal. Chem.*, **57**, 2007 (1985)

9. J. V. Watson and M. J. Walport, *J. Immunol. Methods*, **93**, **171** (1986)

10. R. A. Mathies and L. Stryer, *Applications of Fluorescence in the Biomedical Sciences*, Alan R. Liss, Inc., New York, 1986, pp 129-140.

11. D. C. Nguyen, R. A. Keller, J. H. Jett, and J. C. Martin, *Anal. Chem.*, **59** 2158 (1987)

12. D. C. Nguyen, R. A. Keller, and M. Trkula, *J. Opt. Soc. Am. B*, **4**, 136 (1987)

13. K. Peck, L. Stryer, A. N. Glazer, and R. Mathies, *Proc. Natl. Acad. Sci. USA*, **86**, 4087 (1989)

14. J. H. Jett, R. A. Keller, J. C. Martin, B. L. Marrone, R. K. Moyzis, R. L. Ratliff, N. K. Seitzinger, E. B. Shera, and C. C. Stewart, *J. Biomol. Struct. & Dynam.*, **7**, 301 (1989)

15. J. H. Hahn, S. A. Soper, H. L. Nutter, J. C. Martin, J. H. Jett, and R. A. Keller, *Appl. Spectrosc.*, **45**, 743 (1991)

16. E B Shera, N K Seitzinger, L M> Davis, R A Keller, and S A Soper, *Chem Phys. Lett.*, **174**, 553 (1990)

17 S A Soper, L M Davis, and E B Shera, *J Opt. Soc Am B*, **9**, 1761 (1992)

18. C W Wilkerson, Jr , P M Goodwin W P Ambrose, J C Martin, and R. A. Keller, *Appl Phys Lett* , **62**, 2030 (1993)

19 S A Soper, Q L Mattingly, and P Vegunta, *Anal. Chem* , **65**, 740 (1993)

20 J Tellinghuisen, P M Goodwin, W P Ambrose, **J. C** Martin, and R A Keller, *Anal. Chem* , **66**, 64 (1994)

21 W B Whitten, J M Ramsey, S Arnold, and B Bronk *Anal Chem* , **63** 1027 (1991)

22. K. C. Ng, W B Whitten, S Arnold, and J M Ramsey, *Anal. Chem* , **64**, 2914 (1992)

23. P A. Johnson, T E Barber, B W Smith, and J. D Winefordner, *Anal Chem* , **61**, 861 (1989)

24 S J Lehotay, P A Johnson, T E. Barber, **J. D**. Winefordner, *Appl Spectrosc* , **44**, 1577 (1990)

25. S J Lehotay, *Ph D Dissertation*, University of Florida, 1992

26 Y H. Lee, B W Smith, and J D Winefordner, **Talk** Presented at the 20th Annual Meeting of the Federation of Analytical chemistry and Spectroscopy Societies, Detroit, Michigan, 1993

27 Y H Lee, B W Smith, and J D Winefordner, Talk Presented at The 45th Pittsburgh Conference Chicago, Illinois, 1994

28 J H Jett, R A. Keller, J C Martin, B L. Marrone, R K. Moyzis, R L. Ratliff, N K. Seitzinger E B Shera, and C C Stewart, *Struc Methods Proc. Conversation Descrit Biomol Stereodyn*., 6 79 (1990)

29 S A. Soper, L M Davis, F R. Fairfield, M L. Hammond, V A. Harger, J H Jett, R.A. Keller, **J C** Martin, H L. Nutter, E.B Shera, and D J. Simpson, *Proc Int. Soc Opt. Eng* , **1435** 168 (1991)

30 G C Saunders, J H Jett, and J C Martin, *J. Clin. Chem.* **31**, 2020 (1985)

31. A. Feinstein, D. Beale, *Immunochemistry: An Advanced Textbook.*, John Wiley & Sons, pp263-306, 1977

32. M. Novotny, *Anal. Chem.*, **53**, 1294A (1981)

33. J. Ruzicka, *Anal. Chem.*, **55**, 1040A (1983)

34. F. Zarrin and N. J. Dovichi, *Anal. Chem.*, **57**, 2690 (1985)

35. T. A. Kelly and G. D. Christian, *Anal Chem.*, **53**, 2110 (1981)

36. V. L. McGuffin and R. N. Zare, *Appl. Spectrosc.*, **39**, 847 (1985)

37. J. N. Demas and R. A. Keller, *Anal. Chem.*, **57**, 538 (1985)

38. R. E. Russo and G. M. Hieftje, *Anal. Chem. Acta*, **134**, 13 (1982)

39. R. Indralingam, J. B. Simeonsson, G. A. Petrucci, B. W. Smith, and J. D. Winefordner, *Anal. Chem.*, **64**, 964 (1992)

40. M. J. Pelletier, *Appl. Spectrosc.*, **47**, 69 (1993)

41. H. Kaiser, *Two Papers on the Limit of Detection of a Complete Analytical Procedure*, Jaifner Publishing, New York, 1969

42. J. D. Winefordner, G. A. Petrucci, C. L. Stevenson, and B. W. Smith, *J. Anal. At. Spectrom.*, **9**, 131 (1994)

43. J. D. Winefordner and C. Stevenson, *Spectrochim. Acta*, **44B**, 757 (1993)

44. C. Th. Alkemade, *J. Appl. Spectrosc.*, **35**, 1 (1981)

45. C. Th. Alkemade, In *Analytical Applications of Lasers*, ed. E. H. Piepmeier, Wiley Interscience, New York, ch. 4 (1986)

46. C. L. Stevenson and J. D. Winefordner, *Appl. Spectrosc.*, **46**, 715 (1992)

47. C. L. Stevenson and J. D. Winefordner, *Appl. Spectrosc.*, **46**, 407 (1992)

48. C. L. Stevenson and J. D. Winefordner, *Appl. Spectrosc.*, **45**, **1217** (1991)

49. R. A. Mathies, K. Peck, and L. Stryer, *Anal. Chem.*, **62**, 1786 (1990)

50. A. P. Larson, H. Ahlberg, and S. Folestad, *Appl. Opt.*, **32**, 794, (1993)

51. R. Mathies, A. Oseroff, and L. Stryer, *Proc. Net. Acad. Sci. USA*, **73**, 1, (1976)

52 J. C. White and L. Stryer, *Anal. Chem.*, **161**, 442, (1987)

53. J. D. Ingle, Jr. and S. R. Crouch, *Spectrochemical Analysis*, Prentice Hall, Englewood Cliffs, New Jersey (1988)

54 T. Imasaka, A. Yoshitake, and N. Ishibash, *Anal. Chem.*, **56**, 1077 (1984)

55 T. Imasaka, A. Yoshitake, K. Hirata, Y. Kawabata, N. Ishibashi, *Anal. Chem.*, **57**, 947 (1985)

56. K. Sauda, T. Imasaka, and N. Ishibashi, *Anal. Chem.*, **58**, 2649, (1986)

57. T. Imasaka, A. Tsukamoto, and N. Ishibashi, *Anal. Chem.*, **61**, 2285, (1989)

58 D. A. Wilberforce, G. Patonay, *Spectrochim. Acta*, **46A**, 1153 (1990)

59 T. Imasaka and N. Ishibashi, *Anal. Chem.*, **62**, 363A, (1990)

60 T. Higashijuma, T. Fuchigami, T. Imasaka, and N. Ishibashi, *Anal. Chem.*, **64**, 711, (1992)

61. G. Patonay and M. D. Antoine, *Anal. Chem.*, **63**, 321A, (1991)

62. N. J. Dovichi, J. C. Martin, J. H. Jett, and R. A. Keller, *Science*, **219**, 845 (1983)

63 P. A. Jansson and C. L. Korb, *J. Quant. Spectrosc. Radiat. Transfer*, **8**, 1399 (1968)

64 J. Puerta and P. Martin, *APPl. Opt.*, **20**, 3923 (1981)

65 J. Puerta and P. Martin, *APPl. Opt.*, **20**, 259 (1981)

66. J. R. Beacham and K. L. Andrew, *J. Opt. Soc. Am.*, **61**, 231 (1971)

67. A. M. van der Spek, J. J. L. Mulders, and L. W. G. Steenhuysen, *J. Opt. Soc. Am. B*, **5**, 1478, (1988)

68. A. Gallegar and E. L. Lewis, *J. Opt. Soc. Am.*, **63**, 864 (1973)

69 C. Th. J. Alkemade, T. Hollander, W. Snelleman, and P. J. Th. Zeegers, *Metal Vapors In Flames*, Pergamon Press, Elmsford, NY (1982)

70 T. E. Barber, Ph.D. Dissertation, University of Florida, 1992

71. D. Kales, *Laser Focus World*, pp 70, January, 1993

72. H W Messenger, *Laser Focus World*, pp69, June, 1990

73. J. Hecht, *Laser Focus World*, pp93, October, 1992

74. A. J Alfrey, *IEEE J. Quantum Electron.*, **25**, 760 (1989)

75 J M Eggleston, L. G DeShazer, and K. W. Kangas, *IEEE J Quantum Electron* , **24**, 1009 (1988)

76 W R Rapoport and C P Khattak, *Appl. Opt.*, **27**, 2677 (1988)

77. Schwartz Electronic-Optics, Inc , *Titanium sapphire tunable lasers data sheet* (1990)

78 Spectra-Physics, BeamLok™ 2060 User's Manual, December, 1992

79 Omege Optical, data sheet, 1993

80 W F McClure, *Anal Chem* , 66 43A (1994)

81 M R Melamed, T Lindom, and M L Mendelsohn, eds, *Flow Cytometry and Sorting*, Ch 12, Wiley-Liss, New York, 1990

82 R B Mujumdar, L A. Ernst, S R Mujumdar, and A. S Waggoner, *Cytometry*, **10**, 11 (1989)

83 M D Antoine, S. Devanthan, and G Patonay, *Spectrochim Acta.*, **47A**, 501, (1991)

84 L. A. Ernst, R. K. Gupta, R B Mujunday, and A. S Waggoner, *Cytometry*, **10**, 3 (1989)

85 P Andrews-Wilberforce and G Patonay, *Spectroscim Acta*, **46A**, 1153 (1990)

86. P Andrews-Wilberforce and G Patonay, *Appl Spectrosc.*, **43**, 1450 (1989)

87 S Akiyama, "Near-Infrared Luminescence Spectroscopy", in *Molecular Luminescence Spectroscopy*, Part 3, S. G Schulman, ed , Vol 77, Chemical Analysis Series, John Wiley, New York, 229 (1993)

88 G Patonay and M D Antoine, *Anal. Chem.*, **63**, 321A (1991)

89 G Patonay, Talk at Pittcon Meeting, Chicago, Feburary, 1994

90 R. J Williams, M Lipowska, G Patonay, and L. Strekowski, *Anal Chem.*, **65**, 601 (1993)

91. R C Benson and H A. Kues, *J Chem Eng Data*, **22**, 379 (1977)

92. D J S. Birch, G Hungerford, B Nadolski, R.E. Imhof, and A D Dutch, *J Phys E : Sci Instrum* , **21**, 857 (1988)

93 EG&G SPCM-200-PQ-F830 data sheet, 1993

BIOGRAPHICAL SKETCH

Yuan-Hsiang Lee was born in Taipei, Taiwan, the Republic of China, on August 12, 1963. In 1985, he obtained a Bachelor of Science degree in Chemistry from National Sun Yat-Sen University, Kaohsiung, Taiwan. After a two-year military service ranked as the Second Lieutenant in Chun-Chen Army Preparatory School, in 1987, he was a research assistant at the Institute of Atomic and Molecular Sciences, Academia Sinica, Taipei, Taiwan. In 1990, he entered the Graduate School at the University of Florida, Gainesville, Florida.

I certify that I have read this study and that in my opinion it conforms to acceptable standards of scholarly presentation and is fully adequate in scope and quality, as a dissertation for the degree of Doctor of Philosophy

James D. Winefordner, Chairman
Graduate Research Professor of Chemistry

I certify that I have read this study and that in my opinion it conforms to acceptable standards of scholarly presentation and is fully adequate in scope and quality, as a dissertation for the degree of Doctor of Philosophy

Martin Vala
Professor of Chemistry

I certify that I have read this study and that in my opinion it conforms to acceptable standards of scholarly presentation and is fully adequate, in scope and quality, as a dissertation for the degree of Doctor of Philosophy

Robert T. Kennedy
Assistant Professor of Chemistry

I certify that I have read this study and that in my opinion it conforms to acceptable standards of scholarly presentation and is fully adequate, in scope and quality, as a dissertation for the degree of Doctor of Philosophy

Vanessa Young
Associate Professor of Chemistry

I certify that I have read this study and that in my opinion it conforms to acceptable standards of scholarly presentation and is fully adequate, in scope and quality, as a dissertation for the degree of Doctor of Philosophy

Eric R. Allen
Professor of Environmental Engineering Sciences

This dissertation was submitted to the Graduate Faculty of the Department of Chemistry in the College of Liberal Arts and Sciences and to the Graduate School and was accepted as partial fulfillment of the requirements for the degree of Doctor of Philosophy

August, 1994

_____

Dean, Graduate School